CFD Modeling For Entrained Flow Gasifiers In Vision 21 Systems

Michael J. Bockelie
Martin K. Denison, Zumao Chen, Temi Linjewile, Constance L. Senior, Adel F. Sarofim

Reaction Engineering International
77 West 200 South, Suite 210
Salt Lake City, UT 84101

Ph: 801-364-6925
http://www.reaction-eng.com
(bockelie@reaction-eng.com)

The gasification industry has identified improved performance of entrained flow gasifiers as a requirement for Integrated Gasification Combined Cycle (IGCC) power plants to be commercially viable. Recent review papers by [Steigel et al, 2001] and [Holt, 2001a] identified several items that could lead to improved Reliability, Availability and Maintainability of solid fuel gasifiers. Some specific problem spots included fuel injector life, refractory wear, carbon conversion and slag management. Better understanding of how these are impacted by operational changes such as fuel type, slurry content and oxidizer flow would be highly beneficial. Both review papers highlighted the need to make greater use of Computational Fluid Dynamics (CFD) modeling of gasifiers. In the last ten years, CFD modeling has been a key tool in improving the performance of the current fleet of pulverized coal fired electric utility boilers. Likewise, CFD modeling can provide insights into the flow field within the gasifier that will lead to improved performance. An excellent review of recent CFD modeling studies conducted for a wide range of gasifier systems is available in [IEA, 2000].

As part of our DOE Vision 21 project, Reaction Engineering International (REI) is developing a CFD modeling capability for entrained flow gasifiers. Our efforts are focused on two configurations: (1) a single stage, down fired system and (2) a two stage system with multiple feed inlets that could be opposed or tangentially fired. These systems are representative of the dominant, commercially available gasifier systems [NRC,1995], [Holt, 2001b]. The single stage gasifier contains a single fuel injector, located along the gasifier centerline, through which fuel, an oxygen stream and possibly steam are injected. The two stage gasifier consists of two sections connected by a diffuser. Each section can have two or four feed injectors. The first stage is a slagging combustor used to separate the ash from the slag and to provide hot gases to the second stage. Char escaping from the gasifier can be separated from the solids downstream and recycled to the first stage. Additional coal and oxidant can be injected into the second stage where the additional fuel is devolatilized and partially gasified. For both classes of gasifiers hot mineral matter is deposited on the wall as slag. The slagging behavior is a critical to protecting the refractory-lined walls of the gasifier from the harsh environment within the gasifier. Inadequate slagging can lead to excessive refractory wear. However, too much slag can also adversely impact gasifier performance. At present, commercial sized gasifiers used for power generation do not achieve complete carbon conversion of solid fuel with only a single pass through the gasifier. An example of a commercial sized single stage, downfired gasifier is the Texaco

gasifier used at the Polk Power station. Some examples of commercial sized two stage gasifiers are the opposed fired E-gas gasifier used at the Wabash River plant and the air blown, tangentially fired systems being developed in Japan by Mitsubishi.

The gasifier models are being constructed using *GLACIER*, an in-house comprehensive, coal combustion and gasification modeling tool that has been used to simulate a broad range of coal and fossil fuel fired systems. As described below, our model tool is being enhanced in order to account for high pressure effects on the reaction kinetics, high particle loading, and slagging walls. Although our focus is on oxygen blown, pressurized systems, the same model could be used for air blown and/or atmospheric systems. In final form, the gasifier models will provide a tool that can be used to address a broad range of gasifier issues, including syngas composition / quality (including tars), carbon content in the flyash and slag, temperature distribution in the gasifier, slag management, pressure scaling, refractory wear and wall heat transfer.

In this paper we describe the current status of our CFD based modeling tool for entrained flow gasifiers. A brief overview of the basic CFD model is provided, followed by detailed discussions on reaction kinetics and the slagging wall model. Results from parametric studies to explore the impact on gasifier performance (syngas quality and carbon conversion) for different operating conditions are provided.

GASIFIER MODEL DESCRIPTION

The *GLACIER* CFD code is a comprehensive CFD modeling code that can be used to model a broad range of turbulent reacting flows. It is capable of modeling two-phase fuels for either gas-particle or gas-liquid applications. For establishing the basic combustion flow field, full equilibrium chemistry is employed. NOx, vaporized metals and other trace species for which finite rate chemistry effects are important, but which do not have a large heat release that would impact the flow field, can be computed in a post-processor mode. Turbulence chemistry coupling is accomplished using PDF methods. An important aspect of *GLACIER* is the tight coupling used between the dominant physics for industrial applications: turbulent fluid mechanics, radiation heat transfer, chemical reactions and particle/droplet dynamics.

In the following section we discuss, in order, the basic CFD model, slagging wall model and gasification kinetics.

Basic CFD Model

The REI combustion models employ a combination of Eulerian and Lagrangian reference frames [REI_Models], [Bockelie et al, 1998], [Adams et al, 1995], [Smoot and Smith, 1985]. The flow field is assumed to be a steady-state, turbulent, reacting continuum field that can be described locally by general conservation equations. The governing equations for gas-phase fluid mechanics, heat transfer, thermal radiation and scalar transport are solved in an Eulerian framework. The governing equations for particle-phase mechanics are solved in a Lagrangian reference frame. The overall solution scheme is based on a particle-in-cell approach.

Gas properties are determined through local mixing calculations and are assumed to fluctuate randomly according to a statistical probability density function (PDF) which is characteristic of the turbulence. Turbulence is typically modeled with a two-equation non-linear k-e model that

can capture secondary recirculation zones in corners. The turbulent fluid mechanics and chemical reactions are coupled using progress variables to track the turbulent mixing process. Gas-phase reactions are assumed to be limited by mixing rates for major species as opposed to chemical kinetic rates. Gaseous reactions are calculated assuming local instantaneous equilibrium.

The radiative intensity field is solved based on properties of the surfaces and participating media and the resulting local flux divergence appears as a source term in the gas phase energy equation. Our models include the heat transfer for absorbing-emitting, anisotropically scattering, turbulent, sooting media.

Particle mechanics are computed by following the mean path for a discretized group of particles, or particle cloud, in a Lagrangian reference frame. Particle reaction processes include coal devolatization, char oxidation and gas-particle interchange. Particle reactions based on fuels other than coal can be modeled. The dispersion of the particle cloud is based on statistics gathered from the turbulent flow field. Heat, mass and momentum transfer effects are included for each particle cloud. The properties of the particle cloud are computed from a statistical average over the particles within the cloud. The properties of the local gas field are computed with an analogous ensemble averaging procedure. Particle mass and momentum sources are converted from a Lagrangian to an Eulerian reference frame by considering the residence time of each particle cloud within the computational cells. For applications with especially high particle loading, additional smoothing of the source terms can be applied. The resulting volumetric source terms provide the coupling of the dispersed phase particle mechanics and heterogeneous combustion to the gas phase fluid mechanics.

The solution algorithm for two phase flow employs a series of macro-iterative loops over the particle and gas phases (see Figure 1). Within each gas phase macro-iteration loop, an iterative loop is performed over the governing PDE's for fluid mechanics, "chemistry" (i.e., fuel stream mixture fractions and their variances) and radiative transport in a sequential manner to obtain updated solution values. The number of macro-iterations over the particle phase is dependent on the strength of the two-phase coupling within the reactor to be modeled. The governing equations for the gas phase (momentum, k-e, and other scalar variables) are solved using a pressure-based, segregated variable scheme developed for low speed, variable density flows (SIMPLER). Gas properties are updated by first computing the local turbulent mixing, and then computing the chemical properties of the gas; for computational efficiency, chemical properties are interpolated from equilibrium tables that are parameterized by the local heat loss and fuel mixture fractions. The radiative intensity field is determined using a discrete ordinates method (S4 or S6 approximation). The particle phase is computed by solving an initial value problem for the mean trajectory and dispersion of a cloud of particles. Included in the system of ODE's are equations for: particle momentum; continuity of species; particle energy (including particle radiation, convection and chemical reaction); particle liquid vaporization; particle devolatization; and char oxidation. The governing set of ODE's is solved using a time-accurate predictor-corrector method for stiff ODE's. Overall, this solution method provides a flexible, efficient and robust model for computing turbulent reacting two phase flows.

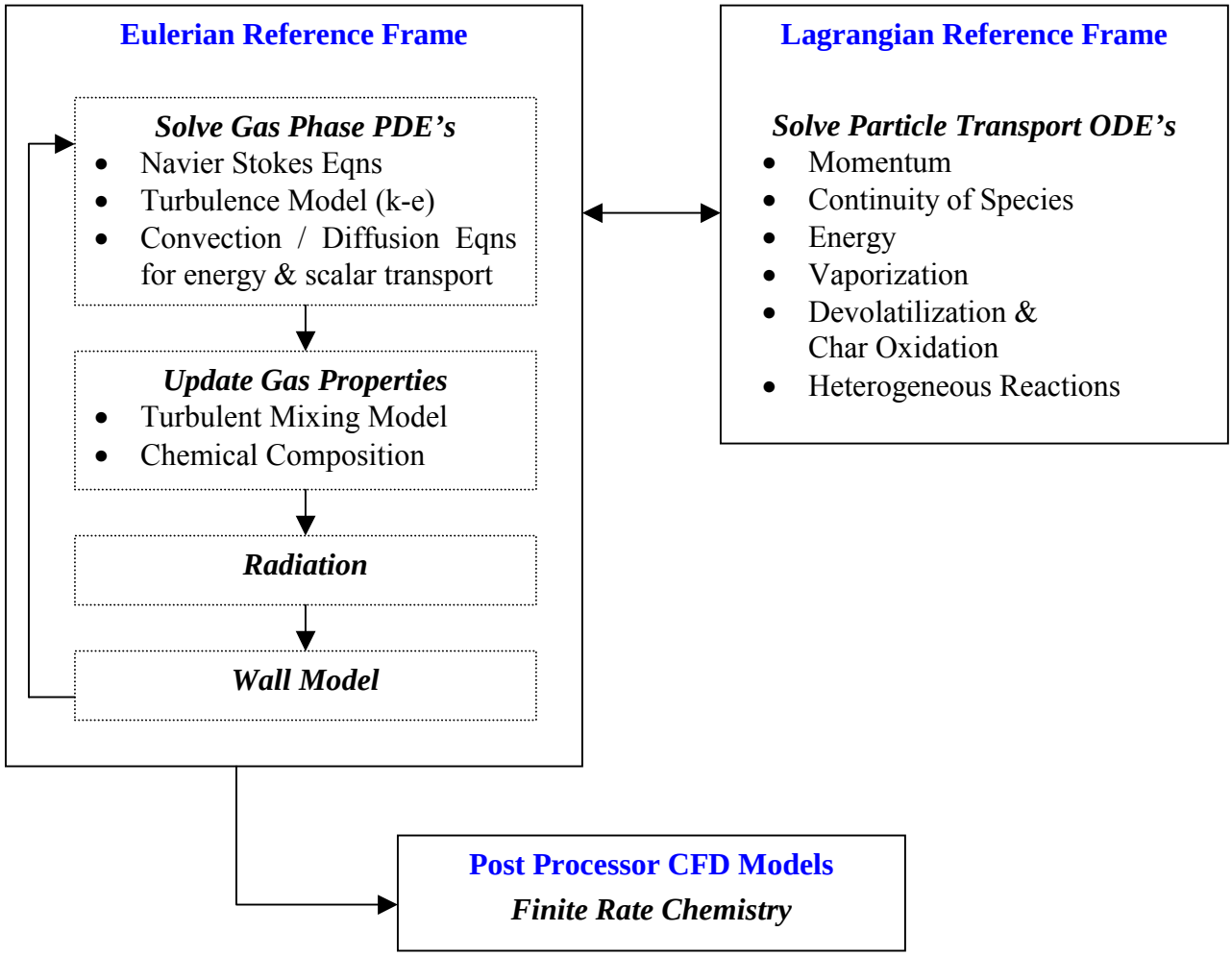

Figure 1. Solution Algorithm

Slagging Wall Model

Slagging of hot mineral matter on the gasifier walls is important for good gasifier operation and thus is included within our comprehensive gasifier model. The slagging wall model we have implemented is an extension of work carried out by Physical Sciences Inc. and United Technologies Research Center under the US Department of Energy's Combustion 2000 program [Senior and Sangiovanni, 2001]; the Collaborative Research Center for Coal and Sustainable Development (CCSD) in Australia [CCSD], most notably Professor Terry Wall, Dr. David Harris and Mr. Peter Benyon; and researchers developing models for the Prenflo gasifier being used at the IGCC plant in Puertollano, Spain [Seggiani, 1998].

The model uses information from the gas flow field in the gasifier (e.g., gas composition, gas temperature, incident heat transfer, and particle deposition rate) to predict the slag properties (e.g., slag flow, slag thickness, frozen ash thickness) and heat transfer through the walls of the gasifier (for an assumed refractory resistance and external ambient temperature). The model is sufficiently general to include the effects of using a cooling jacket/system on the outside of the gasifier. The equations used to describe the ash layer are the conservation equations for momentum, energy, and mass. The model is two-dimensional. The slag thickness is calculated as a function of vertical distance down the walls. At each vertical location, the temperature profile is calculated through the layer thickness. The model is fully integrated into our CFD model of the gasifier. The slagging model can be applied to three-dimensional geometries by applying it for every vertical column of wall computational cells. A more detailed description of the model is provided below.

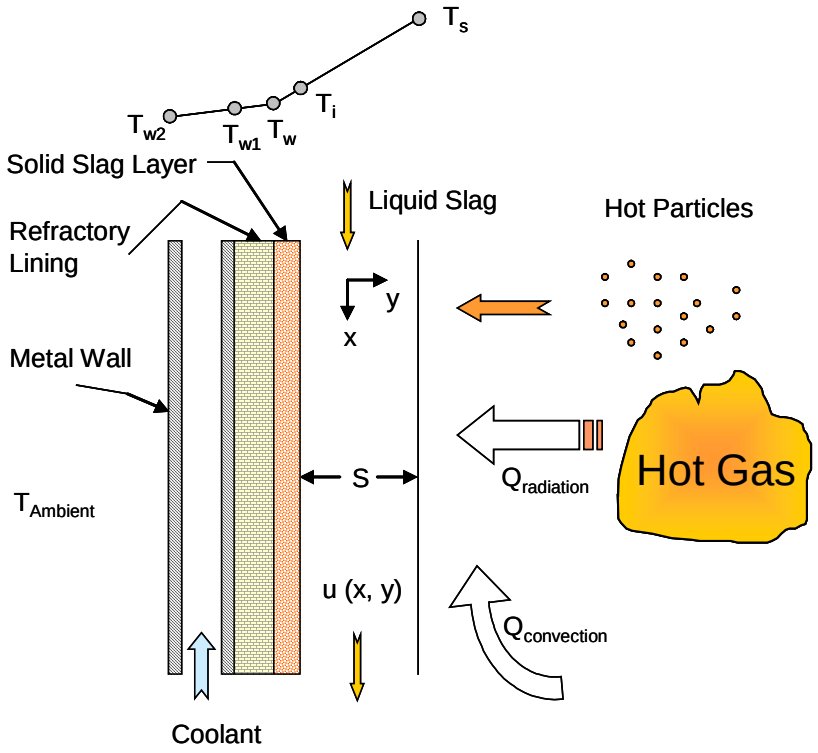

Figure 2. Gravity induced flow of a viscous slag layer down a solid surface.

Model Derivation

The flowing slag model treats the flow of slag on a vertical surface as shown in Figure 2. The equations used to describe the slag layer are the conservation equations for momentum, energy, and mass as first formulated by [Rogers, 1979]. Since inertial forces and the pressure gradient are negligible for a falling film at low Reynolds number with a free surface, the equation of motion (x-direction) for the slag layer is simply

$$\frac{\partial \tau}{\partial y} = \rho g \tag{1}$$

where τ and ρ are the viscous shear stress and mass density of the slag layer, respectively, and g is the gravitational constant. By further assuming that the slag can be represented as a Newtonian fluid, the viscous shear stress for the slag is related to the viscosity, μ, by the expression

$$\tau = \mu \frac{\partial u}{\partial y} \tag{2}$$

where u = u (x,y) is the velocity of the slag layer in the y-direction. The equation of motion can be rewritten as

$$\frac{\partial}{\partial y}\left(\mu \frac{\partial u}{\partial y} \right) = \rho g. \tag{3}$$

Since energy exchange due to convection and viscous dissipation is negligible for low Reynolds number flow and heat conduction across the slag layer is the dominant energy transport mechanism, the energy conservation equation for the slag layer is simply

$$q = k \frac{\partial T}{\partial y} \tag{4}$$

where q = q (x,y) is the heat flux normal to the slag layer, k is the thermal conductivity of the slag, and T = T (x,y) is the temperature of the slag.

The conservation of mass can be expressed as the integral of the velocity profile,

$$\dot{M}_S = \int_0^s \rho u(x,y) dy \tag{5}$$

where $\dot{M}_S$ is the mass flow per unit width of slag layer and the free surface of the slag layer is located at y = s. The mass flux is also equal to the integral of the ash deposition flux from the gas:

$$\dot{M}_S = \int_0^x \dot{m}_S(x) dx \tag{6}$$

where $\dot{m}_s(x)$ is the local ash deposition flux. If the viscosity of a portion of the slag layer is less than the critical viscosity, as indicated by the temperature of the layer, that portion of the layer is assumed to have frozen and the integral of equation (6) is only evaluated across the flowing portion of the slag. The boundary conditions can be stated as:

$$u(x,0) = 0 \tag{7}$$

$$T(x,0) = T_w(x) \tag{8}$$

$$\tau(x,s) = \tau_s(x, T_s) \tag{9}$$

$$q(x,s) = q_s(x, T_s) \tag{10}$$

where T_s is the temperature at the slag surface. Equation (8) assumes that the wall temperature varies axially. Equations (9) and (10) require that we assume a surface shear force, τ_S, and a surface heat flux, q_s, respectively.

A numerical solution was developed for the above set of equations which describe the development, flow, and heat transfer across a falling vertical slag layer. This numerical solution is based on transforming the governing equations with respect to the independent variables of the (x,y) coordinate system as follows:

$$\frac{\partial y}{\partial T} = \frac{k}{q(x,T)} \tag{11}$$

$$\frac{\partial u}{\partial T} = \frac{k\tau}{\mu\, q(x,T)} \tag{12}$$

$$\frac{\partial q}{\partial T} = 0 \tag{13}$$

Examination of equation (11) and the relevant boundary conditions leads to the following result

$$q(x,T) = q_s(x,T) \tag{14}$$

that is, the heat flux through the slag layer is equal to the heat flux at the surface of the layer.

Integration of equation (11) gives the slag layer thickness, s, as

$$s(x) = \frac{k\,(T_s - T_w)}{q_s\,(x, T_s)} \tag{15}$$

To complete the slag layer model, the density, ρ, and thermal conductivity, k, of the slag are assumed to be constant and the free surface shear force is assumed to be zero, while the viscosity of the liquid slag is assumed to vary with temperature according to the Weymann relation which is expressed as:

$$\mu = A\,T\,e^{B/T} \qquad \text{for } T > T_{cv} \tag{16}$$

where A and B are coefficients for the particular ash. This approach was originally proposed by [Urbain et al.,1981] for the prediction of viscosities of ceramics, glasses and steel slags.

By transformation of the equation of motion, equation (3), using equation (11), and integrating with respect to temperature, one obtains the viscous shear stress in the slag layer given by

$$\tau(x, T) = \frac{\rho\, g\, k(T_S - T)}{q_S(x, T_S)} + \tau_S \tag{17}$$

where $\tau_s = 0$.

Then by substituting equation (17) into equation (12) and integrating again with respect to temperature, the velocity profile for the liquid slag layer is given by

$$u(x, T) = \rho g \left[\frac{k}{q_S(x, T_S)}\right]^2 \int_{T_w}^{T} \frac{(T_S - \theta)}{A\, \theta^n\, e^{B/\theta}}\, d\theta \tag{18}$$

Once the velocity is known, the mass flux can be calculated from equation (5) by the expression:

$$\dot{M}_s(x) = \frac{\rho k}{q_s(x, T_s)} \int_{T_i}^{T_s} u(x, \theta)\, d\theta \tag{19}$$

where $T_i = T_w$ if there is no frozen slag layer. Otherwise T_i is assumed to be equal to the temperature of critical viscosity.

In order to complete the description of slag flow behavior in a gasifier, a model describing the interactions between a gravity-induced flow of slag on a hot, vertical wall and heat transfer through the slag layer must take into consideration the viscous behavior of the slag .

Entrained-flow gasification units operate at high temperatures with the hot gases leaving the gasifier in the temperature range 1600 to 1800K for a single stage gasifiers. Because of the high temperatures, mineral matter present in the coal forms slag. The ash slag flows down the refractory walls of the gasifier under the influence of gravity and is removed at the bottom of the gasifier after dropping into a water quench vessel. For these gasifiers to operate well, the slag must be removed continuously. The critical condition for continuous removal of the slag is the maintenance of the slag in a liquid phase so that it can flow unrestrictedly into the slag quench vessel. For this reason slag viscosity is an important property for determination of the performance of a given coal in a gasifier. As such, it is generally accepted that the optimum slag tapping viscosity is in the range 15 – 25 Pa·s at temperatures ranging from 1673 – 1773 K. It becomes apparent therefore, that the molten slag must have a low viscosity for good slag flow at the tapping temperature. The tapping temperature, however, must be high enough so as to avoid crystallization of the slag in the tapping hole but not high enough to have a negative impact on the cold gas efficiency of the gasifier. Therefore the removal of slag from a gasifier depends on the viscosity of the slag and the temperature at which the slag begins to crystallize.

A number of empirical correlations relating the viscosity of a slag to its composition and temperature have been reported in the literature. These include the correlations published by [Reid and Cohen, 1944], [Hoy et al., 1965], [Watt, 1969], [Urbain et al., 1981] and [Schobert et al., 1985] for a variety of operating conditions.

Spurred by the need for prediction of viscosity of slags in entrained flow gasifiers, [Patterson et al., 2001] published an extensive report on the relationship between slag viscosity, ash composition and temperature for Australian coal ashes. The treatise is based on the modified Urbain model which yields viscosity-temperature relationships for gasifier slags with wt % FeO contents in the ranges 0-2.5, 2.5 – 5, 5 – 7.5, 7.5 – 10, 10 – 12.5, 12.5 – 15. In the present work these viscosity models have been incorporated in a CFD code for prediction of gasifier performance. Figures 3 and 4 show a comparison between predicted and experimental slag viscosities. The model considers the composition of the ash to be limited to the weight percent of the major species, namely, SiO_2, Al_2O_3, CaO and F_2O_3. In the model calculations, Fe_2O_3 is converted to FeO in order to account for the reducing environment in the gasifier.

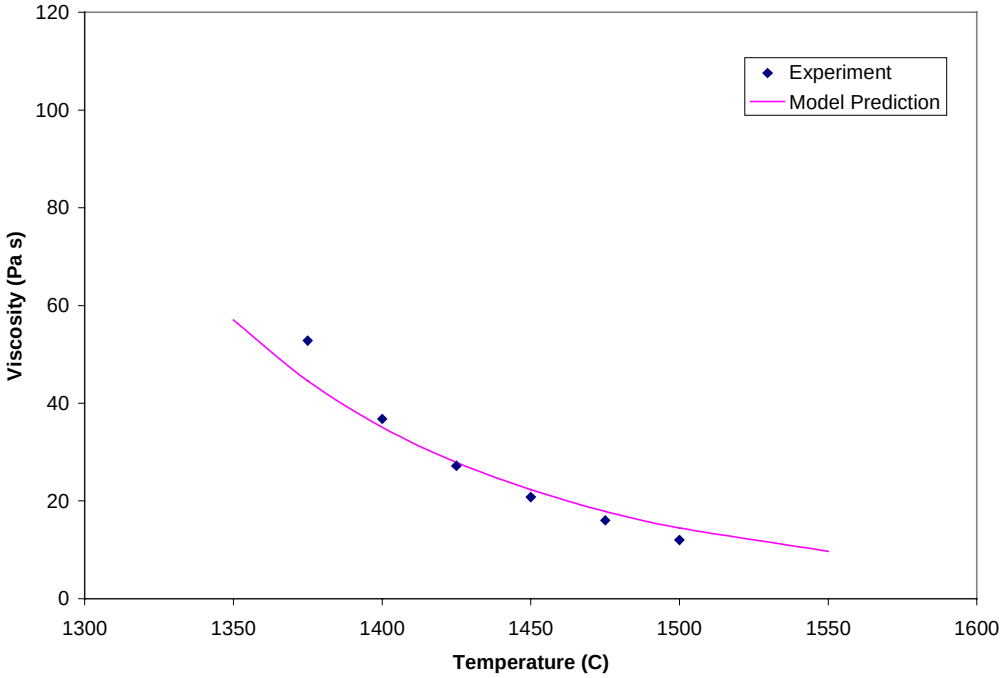

Figure 3. Predicted and experimental viscosities for a coal ash slag containing 52.2% SiO_2, 24.9% Al_2O_3, 4.83% CaO, 8.48% Fe_2O_3.

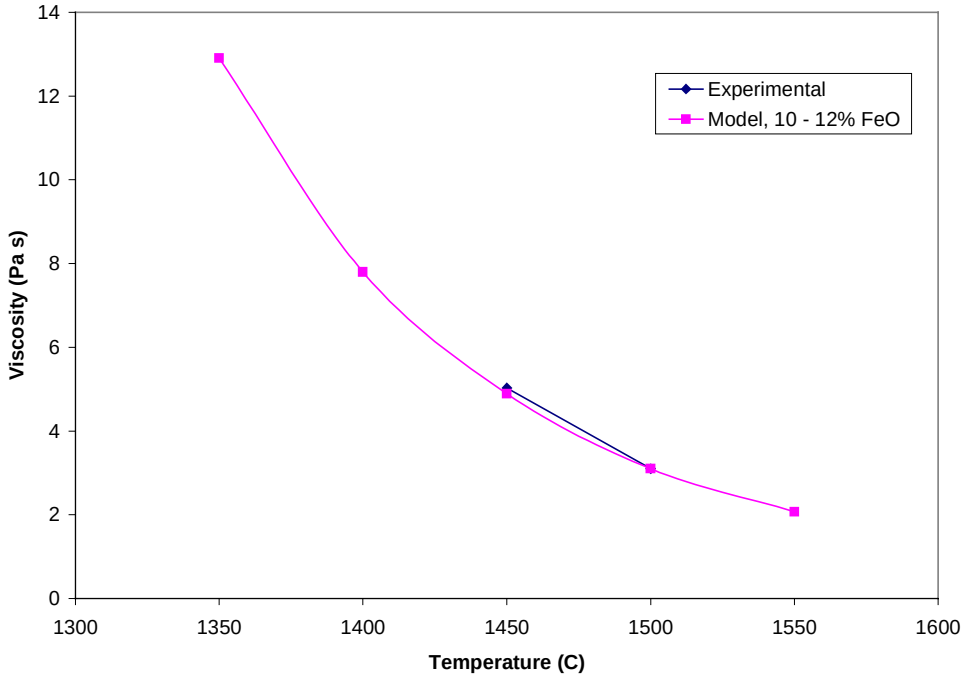

Figure 4. Predicted and experimental slag viscosities at 1723 and 1773 K. Coal ash contains 46.8% SiO_2, 23.16% Al_2O_3, 9.60% CaO and 11.56% Fe_2O_3.

The flow behavior of coal slags has been described in detail by [Watt, 1969]. Briefly, coal slags exhibit Newtonian flow at high temperatures where slag viscosity decreases with increase in temperature. However, if a Newtonian slag is cooled, its viscosity will increase until the fluid transforms to a Bingham plastic. Further slow cooling of the slag below a threshold temperature value will result in a sharp increase in viscosity, caused by the formation of crystals in the liquid. This viscosity is called the critical viscosity. The temperature at which this occurs is the highest temperature at which solid and liquid slag can co-exist in equilibrium and is called the temperature of critical viscosity, denoted by T_{cv}. If the slag is cooled even further beyond T_{cv}, more crystals will separate out and eventually the slag will become a solid.

The temperature of critical viscosity is a function of the ash composition. Estimation of the temperature of critical viscosity is a difficult proposition because a large number of data points covering a wide range of compositions is needed to provide a meaningful correlation. We have developed a correlation for T_{cv} following the procedure laid out by [Hoy et al., 1965] and the slag data of [Patterson et al., 2001] given as

$$T_{cv}[\mathrm{K}] = 3452 - 519.5\alpha + 74.5\alpha^2 - 67.8\beta + 0.86\beta^2 \qquad (20)$$

where $\alpha = SiO_2/Al_2O_3$ and $\beta = Fe_2O_3 + CaO + MgO$

$SiO_2 + Al_2O_3 + Fe_2O_3 + CaO + MgO = 100$ [weight%]

Figure 5 shows the relationship between the T_{cv} correlation and the experimental data of [Patterson et al. , 2001].

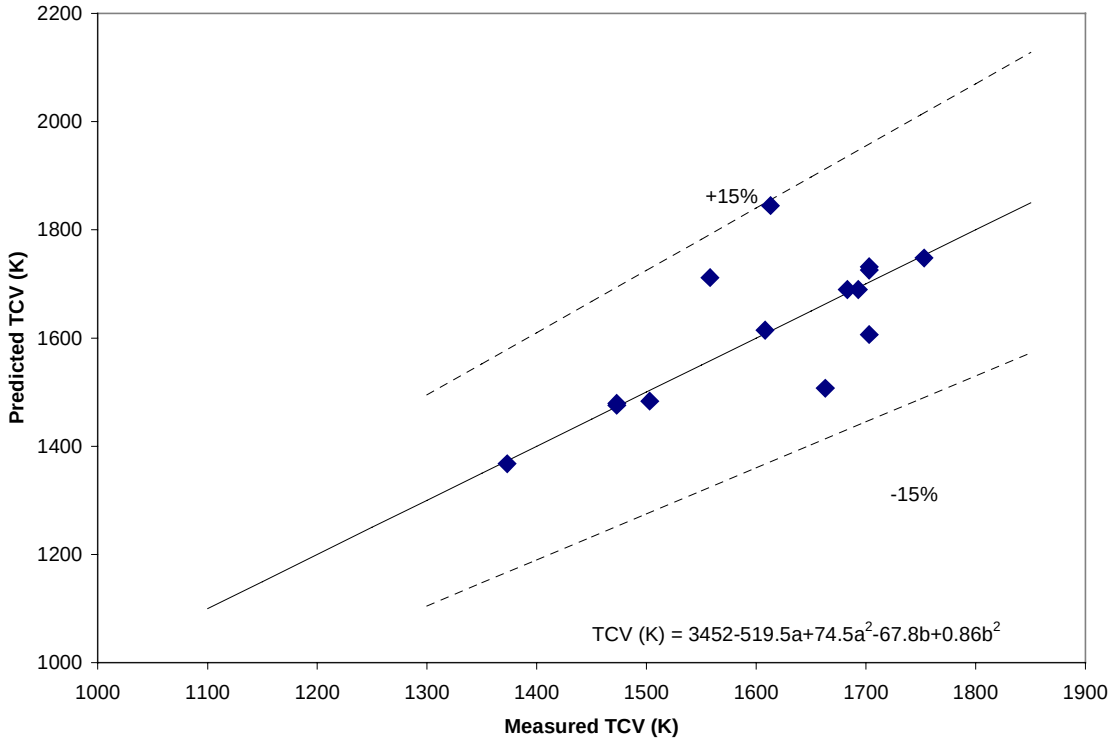

Figure 5. Correlation of predicted and measured temperature of critical viscosity for coal ash slags using experimental data of [Patterson et al, 2001].

Numerical Solution

The numerical procedure developed to simultaneously solve for the net radiant heat transfer to the wall, the liquid slag layer thickness and its related characteristics, at each axial position of the gasifier is as follows;

1. Assume the thickness of the liquid slag layer. At the top of the gasifier, at y = 0, the slag layer thickness is defined to be zero. For y>0, the slag layer thickness at the previous axial position is a good initial assumption for subsequent axial positions.

2. Using an iterative procedure based on the radiation and conduction equations, compute the surface temperature of the slag layer and the net heat flux to the wall slag surface.

3. Compute the velocity profile in the slag layer using equation (18).

4. Compute the mass flux of liquid slag using equation (19).

5. Compute the amount of slag which has frozen, as defined by the portion which is at a viscosity greater than the critical value. The temperature corresponding to the critical viscosity, T_{cv}, is used for this determination of the frozen slag fraction.

6. Compare the mass flux of liquid slag, computed in equation (3), with the sum of the deposition of ash from the gas phase which is in the slag layer, computed in equation (4). If these computed values for the slag mass flux agree within a reasonable tolerance (0.1% should be acceptable), the assumed slag layer thickness is correct.

7. Repeat the above procedure until accurate and consistent values have been found for the slag layer thickness and surface temperature.

CFD Implementation

The above flowing slag wall model has been integrated into the *GLACIER* gasifier model where the inputs (incident heat flux and particle deposition flux) needed for the slagging calculation are taken from the CFD heat transfer and particle calculations. The wall boundary of the gasifier model is divided into vertical strips, a slag calculation is performed as outlined above for each strip. The slag surface temperature solutions are then transferred back to the CFD heat transfer calculations as temperature boundary conditions. Iterations between the CFD and slagging model proceed until convergence.

Model Results

In this section, results for the 2-stage gasifier are presented. Figure 6 shows cross-sectional area averages of liquid and solid slag thickness as functions of the gasifier height. Slag formed only in the combustor section. Liquid slag thickness is in an order of a few millimeters, which is similar to that reported in Benyon et al. (2000), who simulated slag behavior in an air-blown gasifier with a similar geometry as used in this work. Solid slag also formed in the lower section of the gasifier, where the wall temperature changed dramatically, as shown in Figure 7. T_s and T_i in the figure denote liquid slag surface temperature and liquid-solid slag interface temperature, respectively. Figure 8 shows local slag thickness; the horizontal axis represents radial location of the gasifier, starting from the center of one of the injectors in the combustor section and moving counterclockwise. A few vertical strips of liquid slag can be observed; these strips locate above the middle-level injectors. Solid slag mainly formed in the section between the lowest-level injectors and the middle-level injectors, and in a region above the highest-level injectors.

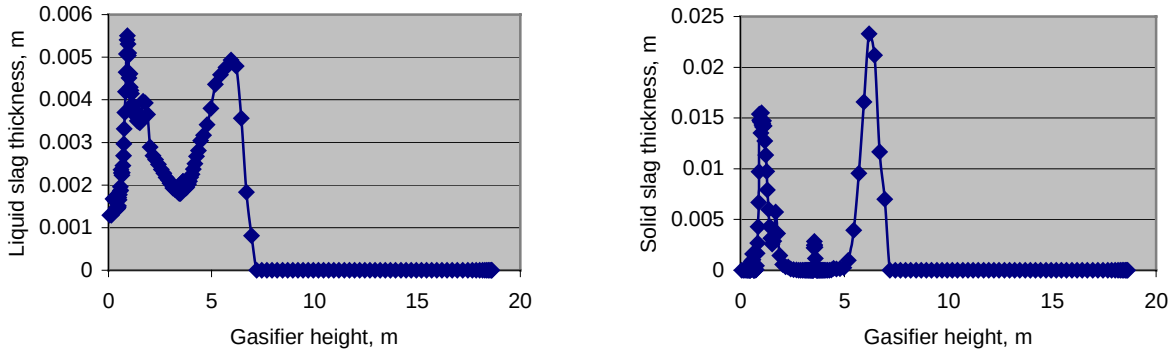

Figure 6. Average slag thickness as a function of gasifier height.

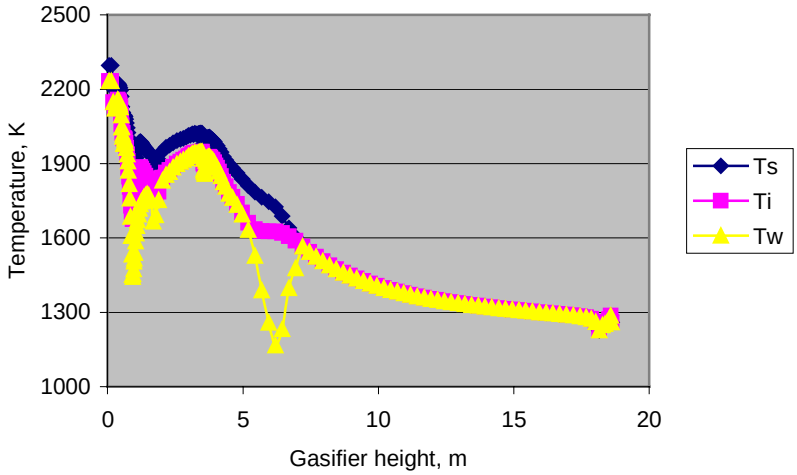

Figure 7. Average liquid slag surface temperature, liquid-solid slag interface temperature and wall temperature as functions of gasifier height.

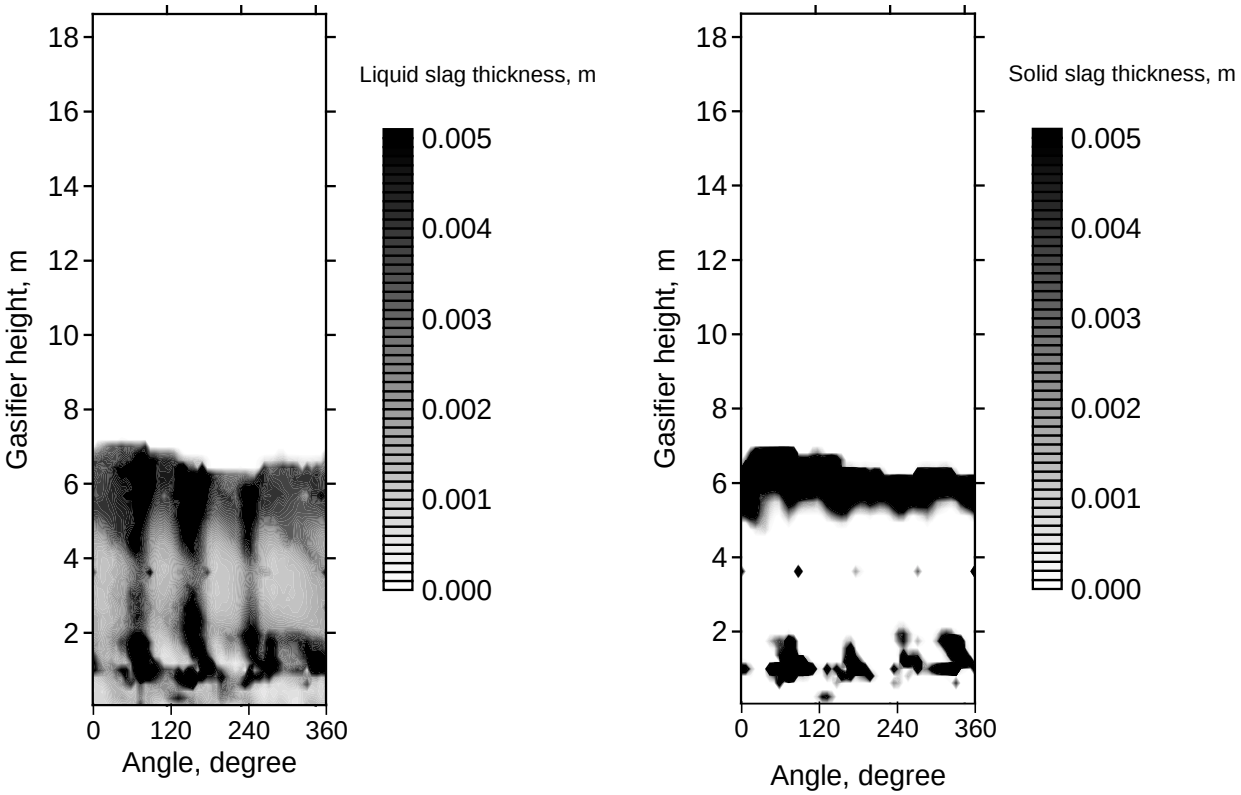

Figure 8. Local liquid and solid slag thickness.

Reaction Kinetics

There is an extensive literature on the kinetics of devolatilization and gasification. Much of it is directed at the early moving bed and fluidized bed gasifiers and therefore is not directly relevant to entrained flow gasifiers, that involve higher temperatures and shorter residence times than packed and fluidized bed gasifiers. The literature on entrained flow gasification is limited; furthermore, some of the gasification kinetics at high pressures have been carried out on char samples generated at atmospheric pressure or slow heating conditions and that are therefore not representative of chars present in entrained flow gasifiers. In the current work, we draw extensively on an ongoing effort on gasification kinetics being carried out in Australia under the directions of Dr. David Harris at the CSIRO and Prof. Terry Wall at the University of Newcastle. The Australian data constitute one of the best sources of information and we have ready access to the information through a Memorandum of understanding between REI and the Collaborative Research Center for Sustainable Development (CCSD).

Devolatilization

Thermal decomposition kinetics is fast at entrained gasification temperatures and is not a strong function of pressure. Volatile yields are suppressed because volatile transport out of coal particles is inhibited as the pressure is increased. Many models have been developed for devolatilization, which give the rate, volatile yield and composition of the products. The three most widely used are these developed by Solomon and co-workers (1988, 1992), Niksa and Kerstein (1991), and Fletcher and Pugmire (1990). The models yield relatively comparable results. We have chosen the Chemical Percolation Devolatilization (CPD) model of Fletcher and Pugmire to provide information of importance to gasification such as tar yields, since it is in the public domain. The model also provides the effect of pressure on volatile yields. The results from the Fletcher and Pugmire model on the effect of pressure on volatile yields is compared in Figure 9 with data and correlations from a number of different investigations.

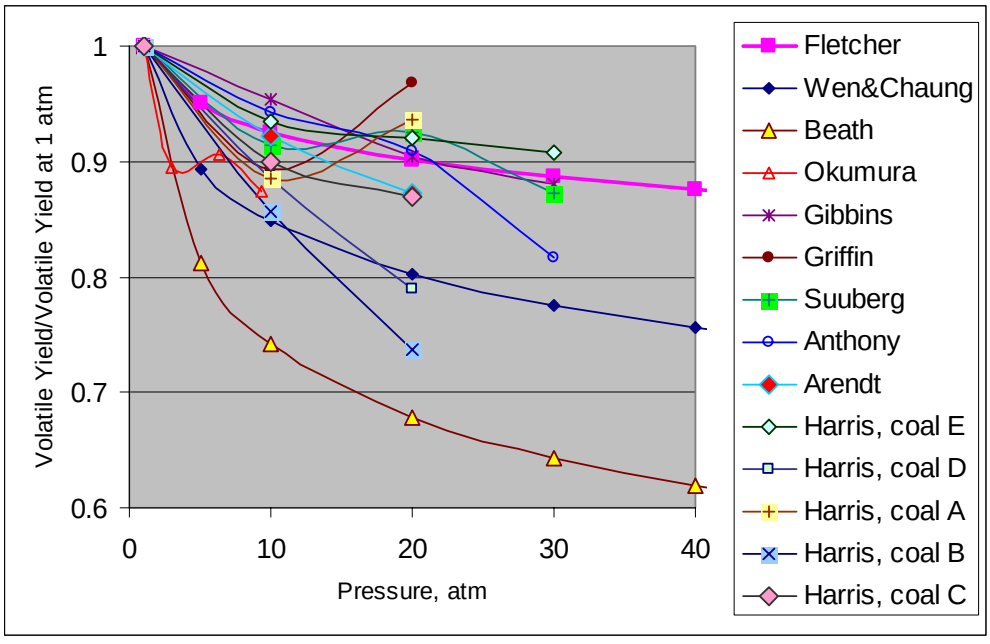

Figure 9. Comparison of model prediction of volatile yields with experimental data.

The CPD model tends to under-predict the decrease in volatile yields with increasing pressure, over a range of pressure from 1 to 30 atm, using a variety of coals. Included in the figure is the correlation by Wen and Chaung (1979), based on the data of Anthony et al. (1976) over the range of 0.1 to 50 atm:

$$\frac{V_p}{V_{p=1}} = 1 - 0.066 \ln P_t \tag{21}$$

where P_t is the total pressure in atmospheres.Wen and Chaung's model slightly over-predicts volatile yields at high pressures. Another correlation, by Beath, significantly over-predicts the effect of pressure on volatile yields. The future studies at the CCSD, involving entrained flow gasification, will help resolve the discrepancies between different correlations.

The two competing reaction pathway developed by Kobayashi et al. (1976) was used to model the gasification kinetics in the CFD code. The input parameters to the code are, however, modified to allow for the above dependence on pressure of volatile yields.

Char Morphology

The more important effect of total pressure on devolatilization is that on the morphology and reactivity of the product char. Because of the inhibition of volatile transport out of particles during devolatilization, the particles produced at high pressures have a higher percentage of particles with large macropores but with less micropores. The chars produced at high pressures contain a high percentage of cenospheric particles, classified as Group I by Wall et al. (2002). They developed a correlation for the effect of pressure on the fraction of particles forming cenosphere, f_{ce}. It is

$$f_{ce} = 0.006 P_t + 0.0053 vitr + 0.37 \tag{22}$$

where P_t is the total pressure in atmospheres and *vitr* is the volume percentage of vitrinite content of coal. For a gasifier operated at 25 atmospheres with a bituminous coal having 80 percent vitrinite, all of the particles are predicted to be present as cenospheres. For a lower vitrinite content of 50 percent, again at 25 atmospheres, 75 percent of the particles are predicted to be present as cenospheres. The increase in cenosphere content with increasing pressure increases the char fragmentation during gasification with an attendant increase on char reaction rates (Benfell et al., 2000) and a decrease in the particle size of ash produced (Wu et al., 2000).

The microporosity and therefore total surface area of the char are also impacted by the increase in total pressure. These changes in surface area and porosity will also influence the high pressure reactivity of the chars (Benfell et al., 2000). A further complication on structure is provided by the annealing and deactivation of the carbon structure with increasing exposure to high temperatures (Hurt et al., 1998; Seneca et al., 1998). Such deactivation needs to be considered at the longer residence times in the two-stage gasifier and potentially for char that is recycled.

Kinetics of Char Gasification

Having the correct gasification kinetics is critical for any gasifier model. Kinetics are needed to size the gasifier/combustor and determine the char combustion efficiency and possible char recycle requirements. The three reactants of importance are O_2, H_2O, and CO_2, with the possible addition of H_2 that can contribute to the formation of CH_4 at high pressures. The kinetics are determined by three resistances, that of external diffusion of the gas phase reactants to the particle surface and diffusion of the reactants from the surface, diffusion through the porous structure of the char, and reaction at the internal (mostly) and external char surface.

The external rate of diffusion is given by (Smith, 1982),

$$R_D = 0.75 D_i \left(\frac{P_0}{P_t}\right)\left(\frac{T_m}{T_0}\right)^{1.75} \frac{(C_i - C_s)}{d_p} \tag{23}$$

where the diffusion rate is in kg/m^2.s, T_m is the average temperature of the boundary layer around the particle, and the subscript 0 denotes the reference conditions. For P_0 = 1 bar and T_0 = 1500 K, $D_i = 3.1\times10^{-4}$ m^2/s for O_2. C_i, C_s, and d_p in the above equation are the reactant concentrations in the gas phase and particle surface and the particle diameter, respectively.

The reaction at the internal char surface, called the intrinsic kinetics, is a more fundamental property of the char as it permits the calculation of the effects on total reaction of changing char structure and surface area. Values for the intrinsic rate for a range of pressures are given by the Australian researchers (Benfell et al., 2000; Roberts and Harris, 2000), together with models on how the rates can be converted to the effective surface rate (Liu et al., 2000). One of the advantages of the more fundamental rate expression is that it can permit the determination of the effect of the change in internal pore structure with conversion. Such models have been used to determine the change of reactivity with changing conversion, where there is an initial increase in rate with conversion as the result of the increase in surface area as pores enlarge, followed by a decrease as pores overlap [Liu, et al., 2000].

The intrinsic kinetics that need to be used in such models are complicated by the adsorption/desorption kinetics at sites with a range of activities. The Langmuir-Hinshelwood model is found to still provide a simple representation of the competition of different reactants with the surface. For the CO_2-char reaction, for example, it provides the following relationship for the reaction rate

$$R_c = \frac{k_a p_{CO_2}}{1 + k_b p_{CO_2} + k_c p_{CO}} \tag{24}$$

The denominator represents the inhibition of the reaction as a result of adsorption on reactive surface sites by reactants and products. The number of terms in the denominator will increase in a product mixture containing other species that can be adsorbed on surface sites, such as H_2O. As a consequence of the inhibiting factor of adsorbed species, the order of the reaction between CO_2 and carbon decreases with increasing pressure (Roberts et al, 2001). This is a reason,

additional to the changes in char morphology with pressure, that it is difficult to extrapolate kinetics from atmospheric to higher pressures.

The intrinsic reaction rates of oxygen with carbon can be factors 10^3 to 10^5 higher than those of H_2O and CO_2 [Harris and Smith, 1990; Roberts and Harris, 2000], but these differences decrease to factors less than ten at the higher temperatures in oxygen-blown gasifiers since the activation energies for CO_2 and H_2O are higher than those of O_2 (see Figures 10 and 11). When allowance is made for diffusion within pores and in the particle boundary layer, the differences between the rates of the exothermic O_2/C reaction and the endothermic CO_2/C and H_2O/C become much smaller. But it is usually the case that the reaction of oxygen with carbon precedes those of CO_2 and H_2O.

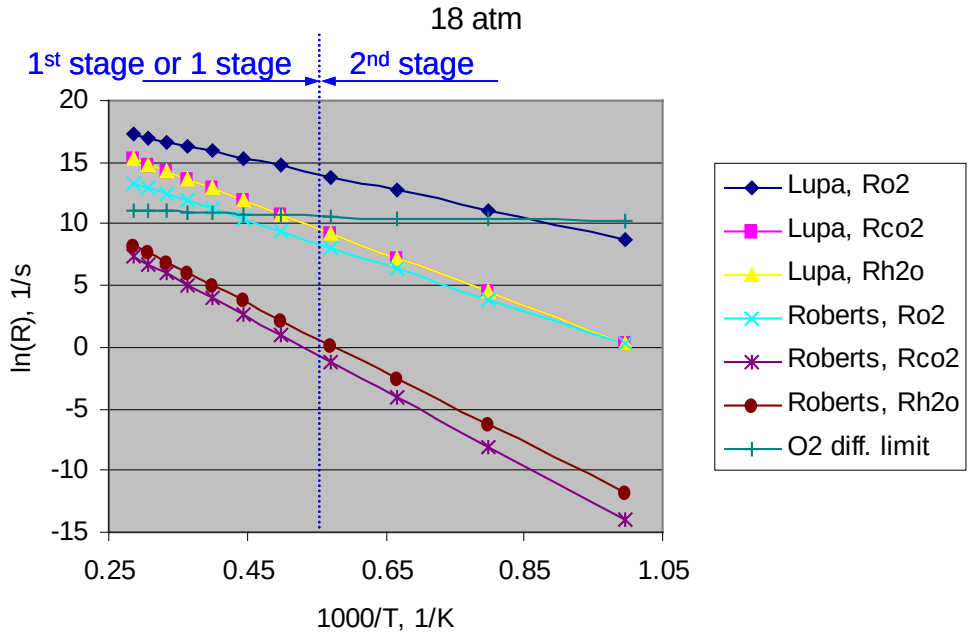

Figure 10. Comparison of the rates at 18 atmospheres from Lupa et al. (1979) and Roberts and Harris (2000) for the apparent reaction rates of O_2, CO_2, and H_2O (each with a mole fraction of 0.2) with the mass transfer controlled rate for oxygen (also with a mole fraction of 0.2).

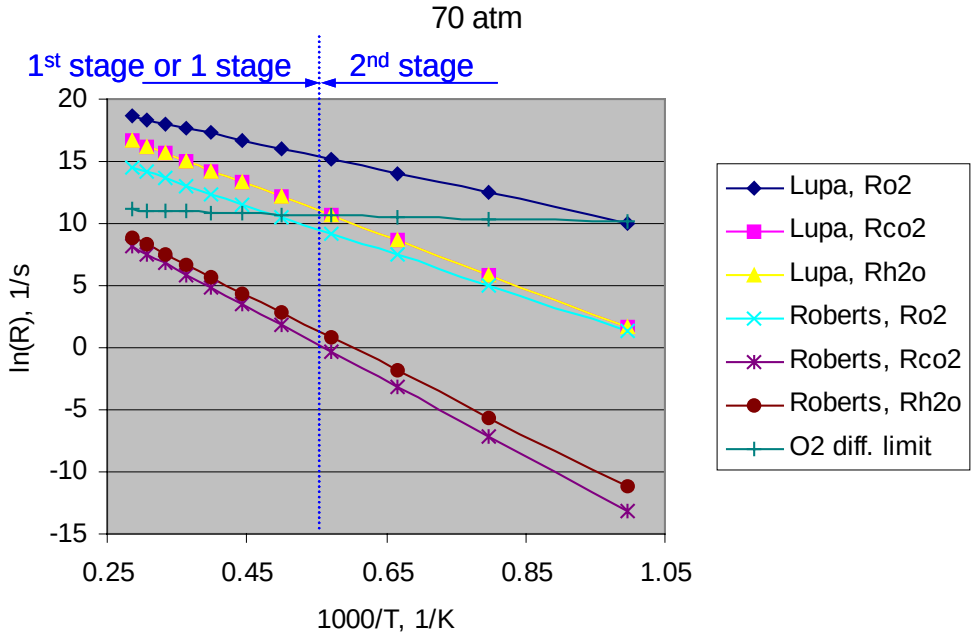

Figure 11. Comparison of the rates at 70 atmospheres from Lupa et al. (1979) and Roberts and Harris (2000) for the apparent reaction rates of O_2, CO_2, and H_2O (each with a mole fraction of 0.2) with the mass transfer controlled rate for oxygen (also with a mole fraction of 0.2).

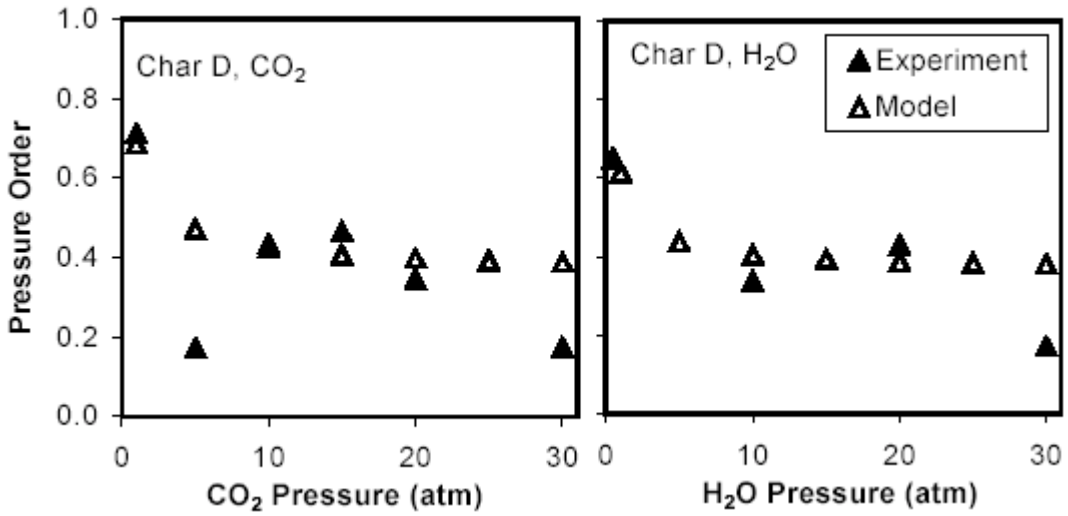

Figure 12. The effect of pressure of gasification gas on the parent order n_i for CO_2 and H_2O (Roberts et al., 2001). Comparison of theoretical values (open triangles) with data (closed triangles).

The intrinsic kinetics can be combined with pore diffusion models to obtain the reaction of a particle or derive reactivity per unit external surface area of a particle the so-called apparent reactivity. Data obtained on particles are often correlated in terms of the apparent reactivity. A commonly used correlation used for chemical kinetics is the

$$R_s = k_i P_{si}^{n_i} e^{-E_i/RT} \tag{25}$$

where the rate constant k_i, activation energy E_i, and reaction order n_i include the complexity of the internal diffusion and therefore may vary with extent of reaction, and the exponent n_i includes the effects of partial pressures P_{si} of other species at the particle surface and therefore also applies only over a limited range of pressures and gas concentrations. Examples of the dependence of the reaction order on pressure are given for the case of the H_2O/carbon and CO_2/carbon reactions in Figure 12. The reaction orders n_i are seen to decrease from around 0.7 at one atmosphere to less than 0.2 at 30 atmospheres. The open symbols represent predictions of n_i for CO_2 and H_2O based on a model of the saturation of surface sites (Roberts et al., 2001).

The simplified correlation of rate given by equation 25 is the one that has been adopted for the CFD models of a gasifier. The rate parameters can be determined either directly from measurements or from intrinsic reactivities employing a pore model to allow for char structure. The kinetic parameters need to cover the temperatures and oxygen concentrations along different trajectories and will therefore be necessary for environments ranging from nearly pure oxygen near the injector to gasification products (see Table 1 for representative values) near the completion of gasification, temperatures up to 1873 K (2912°F), and pressures of to 8 MPa (~80 atmospheres). In order to calculate the rate, one needs to first obtain the concentration of the reactants at the surface, by equating the rate of diffusion to the surface, by equating R_D from equation 3 to R_s from equation 25 and solving for P_{si}, remembering that C_{si} is equal to P_{si}/RT.

In order to provide indications of the relative importance of R_s and R_D, rates have been calculated for pressures up to 80 atmospheres, and temperatures of 1600 to 3000 K for a single stage gasifier (or first stage of a two-stage gasifier), and down to 1100 to 1300 K for the second stage of a two-stage gasifier. Since the rates can be retarded by combustion products the composition of the residual gases was obtained by assuming that the oxygen entrained flue gases the composition of which was taken from typical values for dry and slurry feed gasifiers (see Table 1).

Table 1. Representative Gasifier Product Composition for Dry and Slurry Feed.

Component	Dry Coal Feed	H_2O Slurry Feed
H_2	26.7%	30.3%
CO	63.3	38.7
CO_2	1.5	10.8
CH_4	0.0	0.1
H_2S	1.3	1.0
N_2	4.1	0.7
Ar	1.1	0.9
H_2O	2.0	16.5

The apparent rate R_s is expressed in mass/time of a particle per unit mass and therefore has a dimension of reciprocal time. Values of E, k and n from selected references are shown in Table 1. The literature on char oxidation is enormous and these references were selected because the authors had applied the correlations in the modeling of gasifiers.

Table 2. Selected Kinetics for Char Oxidation with O_2

Authors	E, J/mol	**k**	**n**
Banin et al. (1997)	51048	40 kg/(m^2·s)	-
Joutsenoja et al. (1999)	82368	1903 m/s	1
Monson et al. (1995)	$F(P_t)$	$F(P_t)$	0.5
Lupa and Kliesch (1979)	100483	1404 kg/(m^2·s·atm)	1
Otaka et al. (2001)	105000*	95000 1/atm^n	0.75
Benyon, 2002	223000	5.81×10^{10}- 1.02×10^{11} kg/(m^2·s·atm^n)	0.83
Roberts and Harris, 2000	153000	4×10^7 kg/(kg·s·atm^n)	0.85

* E in Otaka et al.'s paper is given as 105,000 J/kmol but this gives too small a temperature dependence. The value was interpreted as being J/mol to bring it into line with the other measurements.

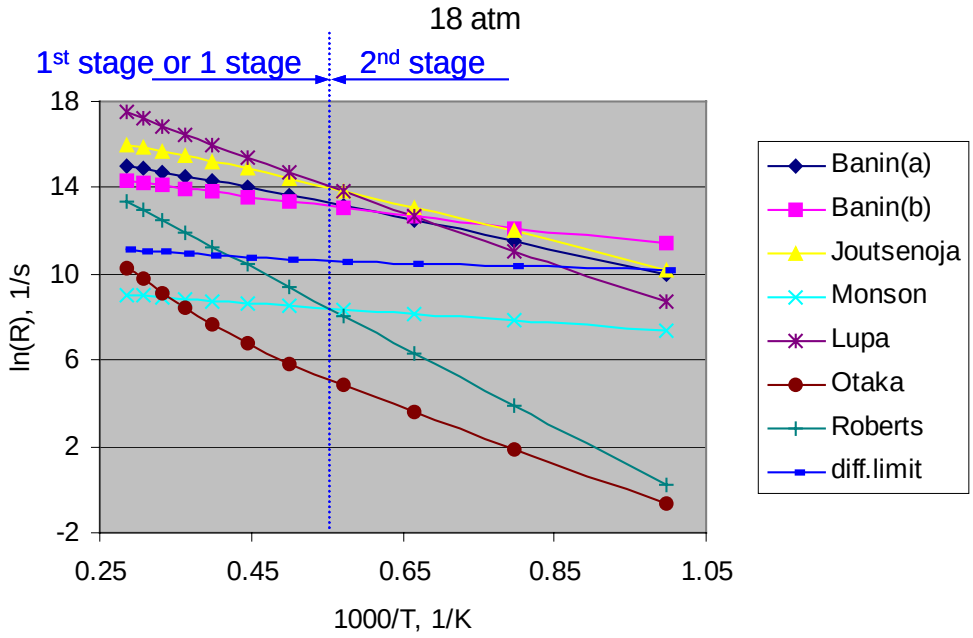

Figure 13. Comparison for a mole fraction of 0.2 oxygen at 18 atmospheres of the apparent kinetic reaction rates from different correlations in the literature with the mass transfer controlled rate.

The importance of a chemical kinetics, R_s calculated from equation 25 with the surface concentration P_{si} equated to the bulk concentration, is compared in Figure 13 with a mass-transfer controlled rate, R_D from equation 23 with C_{si} for the case of reactions at 18 atmospheres with oxygen having a mole fraction of 0.2. There is wide difference in the rates of the different investigators at low temperatures but the data spread is much smaller at the higher temperatures

of interest in the high temperature end. The higher rates, at the temperatures of interest for oxidation in either a single-stage or the first stage of a two-stage gasifier, equal or exceed the mass transfer resistance, with the exception of the results of Monson et al.(1995). As the temperature drops, however, the chemical kinetic rate becomes controlling, underlying the importance of finding good kinetic data on char oxidation.

The rates of gasification with CO_2 and H_2O are compared in Figures 10 and 11 with those for gasification with O_2 for the kinetics Lupa and Kliesch (1979) and Roberts and Harris (2000), at total pressures of 18 and 70 atmospheres. The mole fractions of each oxidation or gasification agent were set to 0.2. The kinetics of the reactions with oxygen are greater than those of CO_2 and H_2O by a factor of one to three order of magnitude over the temperature range of 800 to 2000K with the large differences being at the lower temperatures. At the high temperature end of the gasifier the rates of gasification by CO_2 and H_2O are therefore approaching that of O_2 and can exceed the mass transfer limit. At the low temperatures of the second stage of a two-stage gasifier, the rates of the reactions of gasification with CO_2 and H_2O are much smaller than that of O_2. Since the O_2 concentration in the second stage is small the gasification rate in the second stage will be slow and chemically controlled since the rates shown in Figures 10 and 11 are seen to be lower than the mass transfer limit at the temperature of 1100 to 1350 K, which are typical of the exit temperature of the second stage.

GASIFIER MODEL RESULTS

In this section we describe a series of CFD simulations that have been performed with the gasifier model for the one stage (downfired) and two stage (upfired) "generic" gasifier designs. In this work we do not attempt to optimize the design or operation of a gasifier. Rather, our objective is to exercise the model in order to develop a basis for addressing questions on the reliability of the predicted values and the sensitivity of the model to important model and operational parameters even though these may fall outside the region of practical operating conditions. Simulations targeted toward improving gasifier operation and design will be performed at a later date.

For comparing the predicted gasifier performance we focus on characteristics of the syngas generated, in addition to the basic flow field features. The principle items of interest are the carbon conversion (i.e., % of carbon from the solid fuel converted to carbon in the syngas) and the syngas temperature, composition, higher heating value (HHV, BTU and BTU/SCF) and cold gas efficiency (CGE) which is defined as (from [Benyon et al, 2000]):

$$CGE = (\dot{M}_{syngas} * HHV_{syngas}) / (\dot{M}_{fuel} * HHV_{fuel}) \tag{26}$$

where $\dot{M}_{fuel}$ and $\dot{M}_{syngas}$ are the mass flow rate of the fuel and syngas, respectively, and HHV_{fuel} and HHV_{syngas} are the higher heating value of the fuel and syngas, respectively.

In the following section we discuss, in order, the geometry of the two gasifiers used in this study, the baseline operating conditions, simulation results for the baseline conditions and then a series of parametric simulations that have been performed to evaluate the impact on predicted performance for varying fuel grind, slurry pre-heat, wet and dry fuel feed, system pressure, reaction kinetics, fuel type and gasifier length. Due to complications with implementing the slagging wall model into the CFD code, most of the simulations described below were performed assuming an adiabatic wall boundary condition.

Gasifier Geometry

In general, the internal dimensions of commercial gasifier designs are proprietary information. Hence, the geometry of the gasifiers used in this study are based on a combination of publicly available information (e.g., conference papers, advertising literature, web pages, etc.) and engineering judgment.

The internal shape of the single stage gasifier is based on information for a pilot scale facility [Schneyer et al., 1982] and then scaled for commercial scale systems. For the single stage gasifier (see Figure 14), we assume a L/D ratio of two, where L is the length of the main chamber and D is the internal diameter to the refractory surface. Based on simple plug flow calculations, this results in a gas residence time for the gasifier of about one half of one second. The single stage gasifier contains a single nozzle positioned at the top, center of the reactor through which the oxidant stream and coal-water slurry mixture are injected into the gasifier. The injector is assumed to be an annular nozzle with the oxidant stream passing down a center passage, a slipstream of steam and the slurry is located in an annular passage a small distance from injector centerline. The slurry stream is oriented toward the injector centerline (at the injector tip) that results in a spray entering the gasifier. At the point where injector exhausts into

the gasifier chamber, we assume the coal-water slurry is traveling at about 60 m/s and the oxidant stream is assumed to have a radial profile that has an average velocity of about 100 m/s.

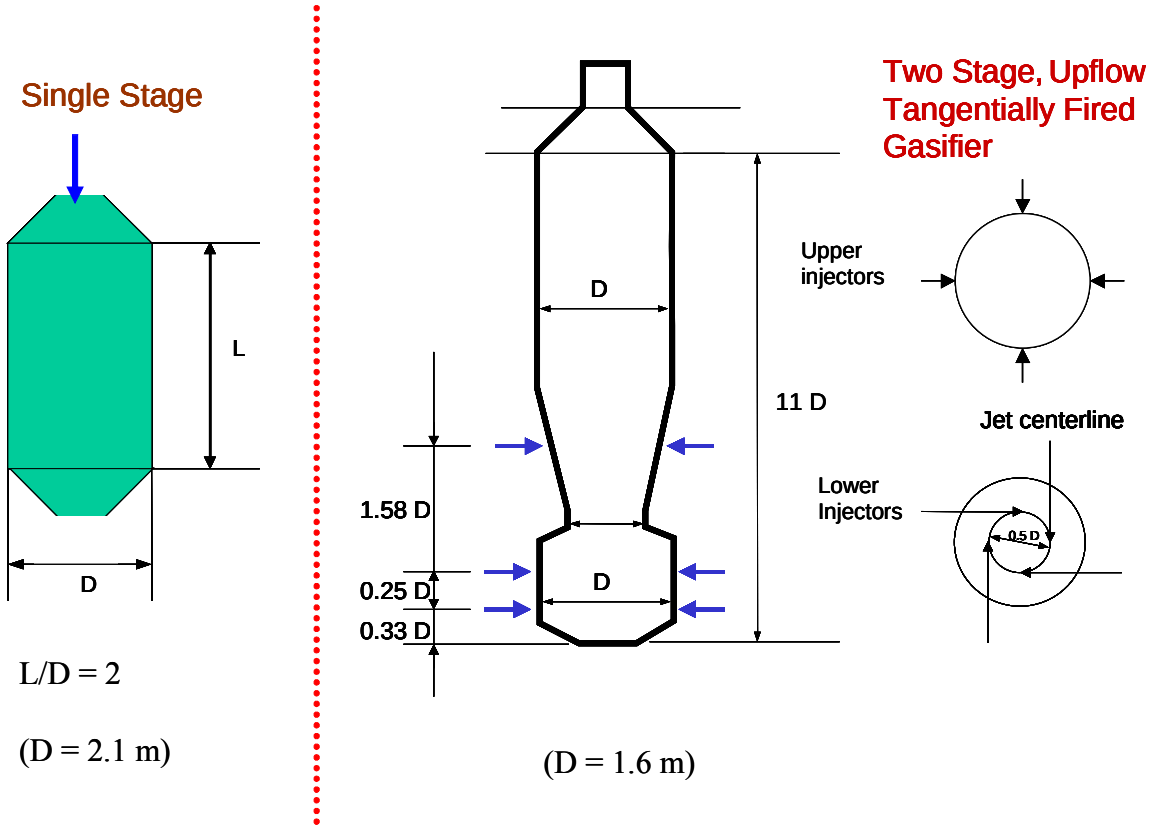

Figure 14. One stage and two stage gasifier geometries.

The shape of the two stage gasifier (see Figure 14) is based on information contained in a series of articles by Chen et al. [Chen et al., 1999], [Chen et al., 2000] that describe modeling studies and scale-up for a pressurized, air blown entrained flow gasifier designed to operate at 2000 tons per day of coal. Additional assumptions used to determine the size of the gasifier were that the gasifier should provide about a two second residence time for the gases (assuming idealized flow) and has a length to diameter ratio (L/D) of about ten. For the two stage gasifier, the length L is based only on the vertical riser section (of constant diameter) and D is the internal diameter of the riser; for the dimensions of the combustion chamber at the bottom of the gasifier engineering judgment was utilized to scale the size information contained in the articles by Chen et al. The two stage gasifier contains three levels of symmetrically placed injectors. The fuel injectors are assumed to have a simple annular passage (concentric pipes) that do not produce a spray action. The bottom two levels of injectors are oriented as per a tangential firing system to create a strong swirling flow field that spirals upward along the axis of the gasifier. The upper level of injectors are oriented opposed to each other.

Baseline Conditions

The baseline operating conditions are taken from a Vision 21 IGCC reference configuration provided by the DOE to Reaction Engineering International for use in our DOE Vision 21 project (see Figure 15). The IGCC reference configuration consists of an entrained flow gasifier, gas clean up system, gas turbines, heat recovery steam generator, steam turbine and SOFC fuel cells.

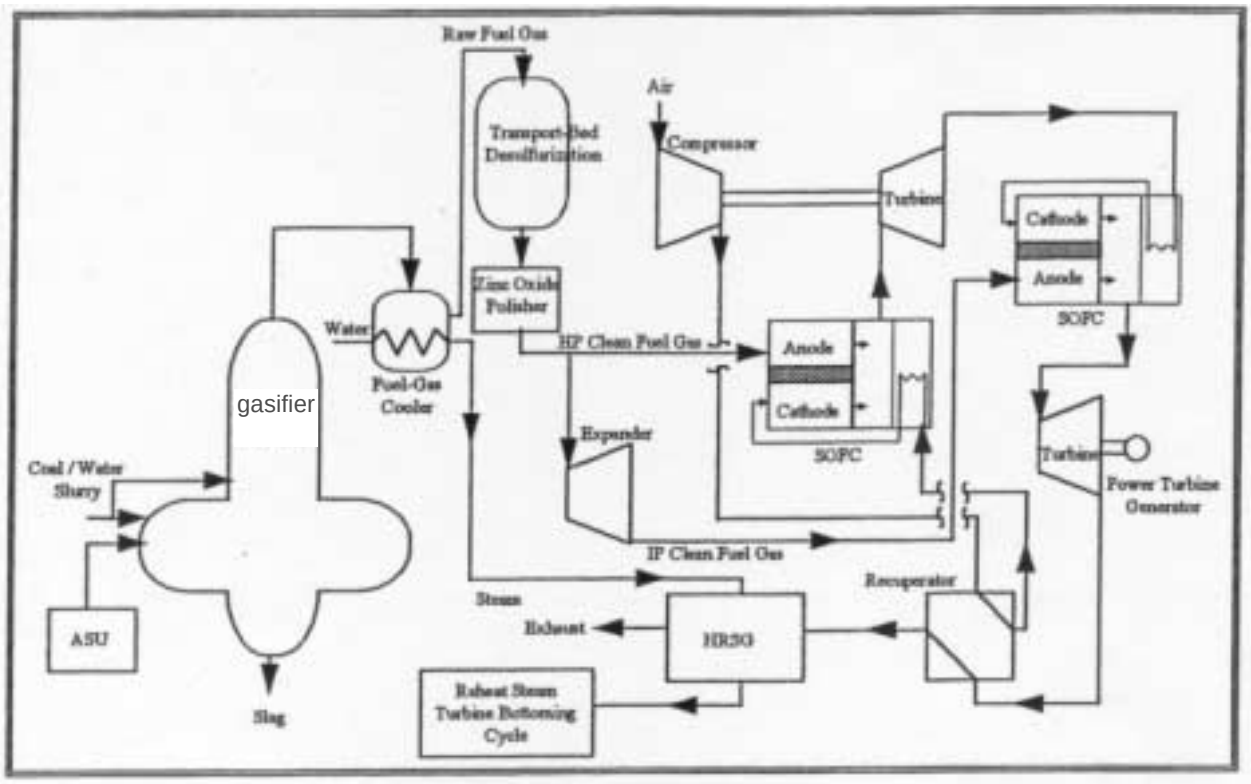

Figure 15. Vision 21 IGCC reference configuration.

Although the reference configuration is based on a two-stage gasifier, we have used the same baseline conditions for testing both classes of gasifier. The key parameters with respect to the gasifier are 3000 tons/day of Illinois #6 coal (see Table 3). For the most of the simulations, we use the kinetic parameters in [Lupa and Kliesh, 1979] which have been derived for Illinois #6 across a range of temperatures and pressures that are representative of gasifier conditions. The system pressure for the gasifier is set at 18atm. The coal-water slurry is 74% solids by weight and the slurry temperature is assumed to be 422 K, or slightly less than boiling at the baseline system pressure. The oxidant stream is assumed to be 95% O_2 and 5% N_2 and to enter the gasifier at a temperature of 475 K. For the two stage gasifier, 78% of the coal and all of the oxidant is uniformly distributed amongst the fuel injectors in the first stage and the remaining coal is uniformly across the injectors in the second stage. Note that there is no oxidant injected into the upper stage. The overall oxygen:carbon (O_2:C) mole ratio is ~0.40, resulting in an overall stoichiomery of about 0.47 and a stoichiometry in the lower stage of about 0.60. A one stage gasifier is typically run at a slightly higher oxidant:carbon mole ratio than is a two stage gasifier. Hence, the baseline simulation has been performed with an oxygen:carbon ratio of 0.50, resulting in an inlet stoichiometry of about 0.54. The operating conditions used in this paper are

very close to the conditions used for the "Hot Gas Cleanup" Aspen simulations contained in [DOE-NETL, 2000a] and [DOE-NETL, 2000b].

Table 3. Fuel properties used for this study

	Illinois #6	Petcoke	PRB coal
Proximate Analysis	As-Received (wt%)	As-Received (wt%)	As-Received (wt%)
Moisture	11.12	7.00	29.00
Ash	9.70	0.52	4.82
Volatile Matter	34.99	12.36	31.38
Fixed Carbon	44.19	80.12	34.80
TOTAL	100.00	100.00	100.00
HHV (Btu/lb)	11666	14282	8618
Ultimate Analysis	As-Received (wt%)	As-Received (wt%)	As-Received (wt%)
Moisture	11.12	7.00	29.00
Carbon	63.75	81.37	50.73
Hydrogen	4.50	2.55	4.23
Nitrogen	1.25	0.92	0.86
Sulfur	0.29	4.81	0.31
Ash	9.70	0.48	4.82
Oxygen (by difference)	6.88	2.87	10.05
TOTAL	100.00	100.00	100.00

Baseline Simulations

One Stage Configuration

Illustrated in Figure 16 is the gross flow field for the one stage gasifier for baseline firing conditions. Shown in Figure 16a is the predicted gas temperature at selected elevations and representative coal particle trajectories, colored by coal volatile content. Illustrated in Figure 16b is the axial velocity at selected elevations and representative coal particle trajectories, colored by coal char content. Overall, the flow field is similar to that of an immersed jet exhausting into a confined volume. There is a core of high velocity, hot gas traveling down the center of the gasifier. Away from the centerline, there exists a slow moving, much cooler reversed flow (i.e., recirculating flow) that travels back toward the injector end of the gasifier. From the particle trajectories it can be seen that the fuel enters the chamber and quickly devolatilizes. Likewise, the fuel initially contains no char, rapidly forms char and then burns out (oxidizes) the char through the remainder of the chamber.

Illustrated in Figure 17 are XY plots showing the gas temperature along the axis of the gasifier. Shown in the temperature plot are the bulk gas temperature, centerline gas temperature, average gas temperature near the wall surface and the average temperature at the wall (or slag) surface. The bulk temperature plot shows a peak value very near the injector, indicating that a large amount of the fuel ignites very soon after entering the gasifier. The peak gas temperature along the chamber centerline does not occur until about one-third of the distance down the gasifier due to the fuel not being the center stream in the fuel injector. The drop in temperature further into the gasifier is due to the endothermic reactions in the gasification reactions. Comparison of the

gas temperature near the wall to the bulk and centerline temperatures emphasizes the severe gradients in the temperature field in the radial direction. In contrast, note that the plots of the near wall gas temperature and wall surface temperature show only a modest change in value along the length of the gasifier.

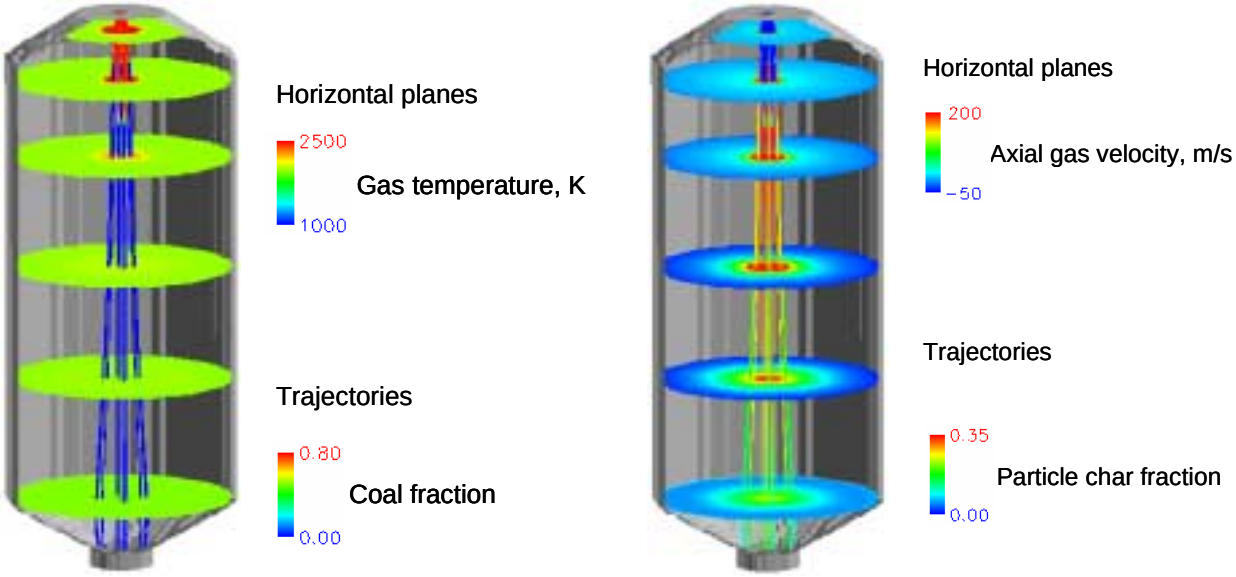

Figure 16. One stage gasifier. (a) Gas temperature and fuel particle coal fraction (left). (b) Gas temperature and fuel particle char fraction.

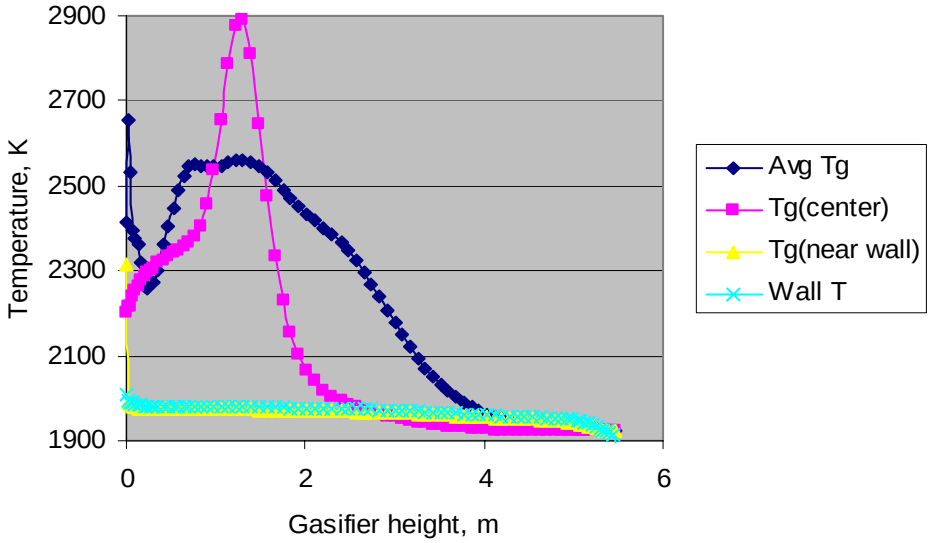

Figure 17. One stage gasifier. Plotted as a function of axial position are the average gas temperature, centerline gas temperature, average gas temperature near the wall and the average wall temperature.

Illustrated in Figure 18a are XY plots for the gas composition along the gasifier axis. The plots show a rapid raise in CO and H_2O content, with the H_2O achieving a peak value at about one-third of the distance down the gasifier, after which both the H_2O and CO_2 content decrease due to the gasification reactions. Shown in Figure 18b are plots of the bulk, centerline and near wall concentration of H_2. Due to the fuel injector configuration, there is no significant H_2 concentration until about one-third of the distance down the gasifier, near where the centerline gas temperature reached a peak value. In contrast, the bulk H_2 concentration shows a very rapid rise in value within a short distance of the injector. Note that the average H_2 concentration near the wall shows almost a constant value throughout the gasifier. Last, all three plots converge to the same value by about two-thirds of the way through the gasifier.

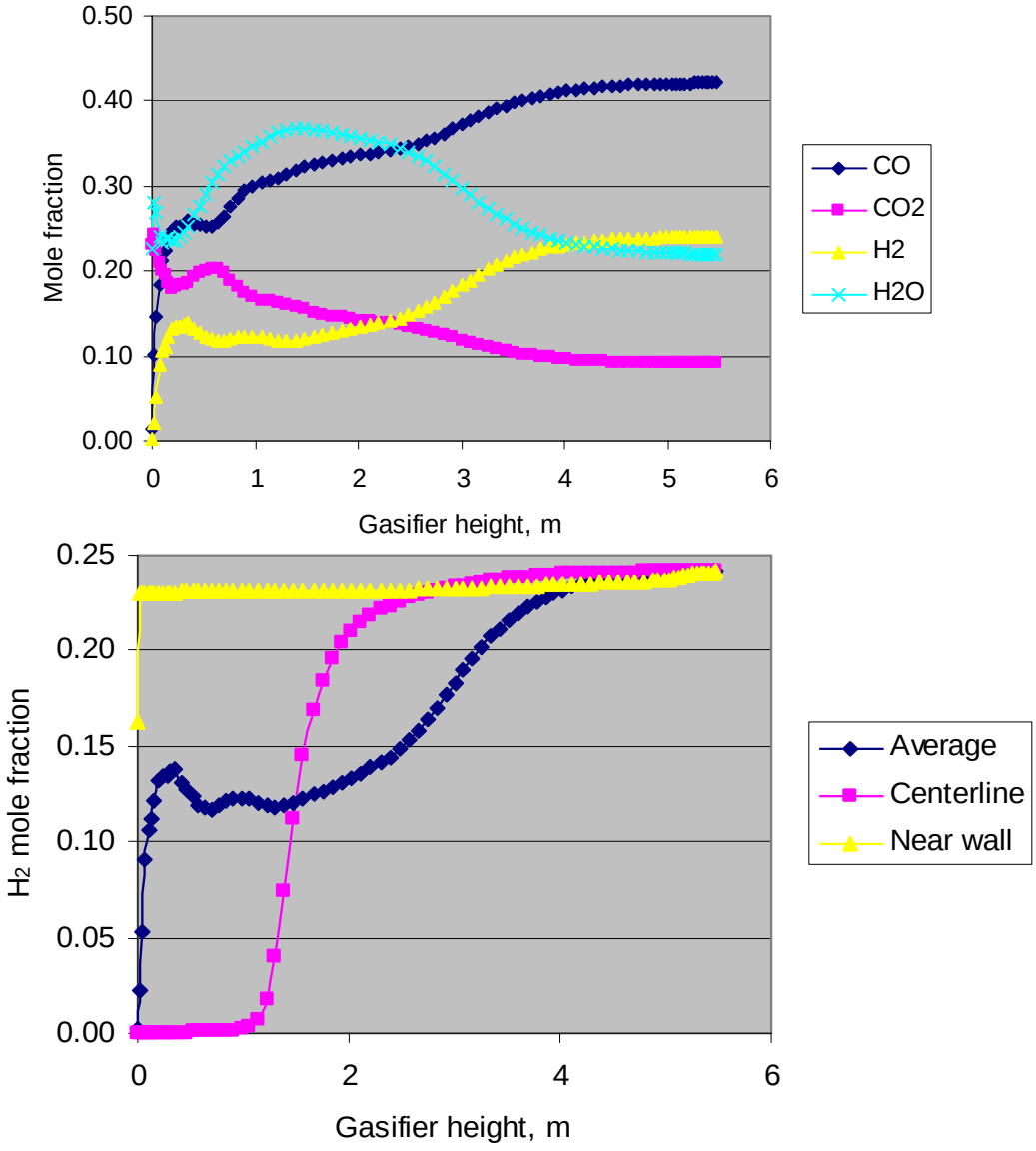

Figure 18. One stage gasifier. Plotted as a function of axial position are (top - a) average concentration of major gas species and (bottom - b) average, centerline and near wall concentration of H_2.

Shown in Table 4 are the average values for the syngas quantity and composition at the gasifier exit. For plant operations the syngas conditions are typically reported on a dry basis for measurements taken at a location downstream of the syngas clean-up system. For simplicity, our results are reported on a wet basis at the model exit plane. From the table it can be seen that for the baseline conditions the model predicts a high carbon conversion (over 97%), cold gas efficiency of slightly more than 75% and a syngas heating value of about 224 Btu/SCF. A DOE funded study that employed an ASPEN analysis for an IGCC plant with a single stage gasifier [DOE-NETL, 2000a] predicted a normalized higher heating value of 240 Btu/SCF for comparable operating conditions (same coal and slurry flow rate, lower oxidant flow rate, higher gasifier pressure) to those used in this simulation. Listed in the table are some reference values for gas, solid and droplet residence times. The Plug Flow Reactor (PFR) residence time provides a reference for the gas residence time and is computed from a single, volume averaged gas density for the reactor and assuming a plug flow; for the given conditions and reactor volume this results in a PFR residence time of about 0.6 seconds. Due to the strong re-circulating flow pattern within the gasifier chamber one must be careful of what is concluded based on the PFR residence. For fuel particles, the model predicts an average residence time of slightly less than 0.03 seconds. For particles, the residence time is defined as the time from when the particle enters the reactor until it impacts on a wall or exits the gasifier. Note that even if the particle "burns out", we continue to track the remaining ash particles until the ash impacts the wall or exits the gasifier. Considering the high velocity flow passing down the center of the gasifier (see Figure 16b), the short residence time of the particles is not unreasonable. For this case, the average residence time for slurry water droplets (i.e., the average time required for a water droplet to evaporate) is about one fifth the residence time of the fuel particles. For many of the parametric simulations that have been performed the droplet residence time changes only slightly where as the residence time of the fuel particles can change significantly.

Table 4. One Stage Gasifier Baseline

Exit Temperature, K	1922.7
Carbon Conversion, %	97.15
Exit LOI, %	18.86
PFR Residence Time, s	0.653
Particle Residence Time, s	0.026
Mole Fraction: CO	0.4217
H_2	0.2413
H_2O	0.2192
CO_2	0.0910
H_2S	0.0079
COS	0.0005
N_2	0.0182
Exit Mass Flow, klb/hr	542.09
HHV of Syngas, Btu/lb	4139.4
HHV of Syngas, Btu/SCF	223.7

Two Stage Configuration

Illustrated in Figure 19 is the gross flow field for the two stage gasifier for baseline operating conditions. To simplify plotting, only the bottom half of the gasifier is included in the figure. Shown in Figure 19a is the predicted gas temperature at selected elevations and representative coal particle trajectories, colored by coal volatile content. Illustrated in Figure 19b is the CO content at selected elevations and representative coal particle trajectories, colored by coal char content. From the figures one can see a strong, swirling flow pattern in the gas flow and the particle trajectories in the lower section. This pattern is to be expected with a tangential firing system used for the lower injectors. Looking at the flow field immediately in front of the top level of injectors the flow pattern changes due to these injectors being oriented opposed to each other. As illustrated by the fuel particle trajectories shown in Figure 19a, the fuel injected into the first stage devolatilizes very quickly but the fuel injected at the top injectors requires a slightly longer time to devolatilize. The char from fuel injected in the first stage gasifies prior to reaching the upper injectors. However, the char in the fuel particles from the upper injectors requires a very long time to fully gasify.

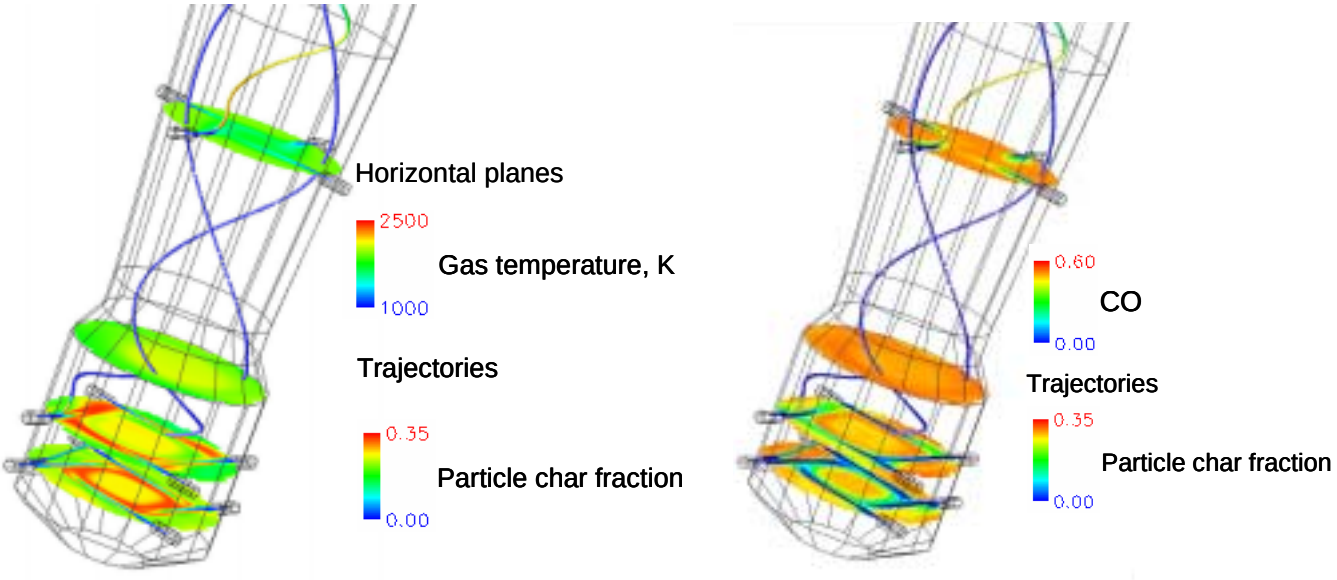

Figure 19. Two stage gasifier. (a) Gas temperature and fuel particle coal fraction (left). (b) CO concentration and fuel particle char fraction.

Illustrated in Figure 20 are XY plots showing the gas temperature along the axis of the gasifier. Shown are the bulk gas temperature, centerline gas temperature, average gas temperature near the wall surface and the average temperature at the wall (or slag) surface. The XY plots are started at 1m. because the complex swirling flow at the very bottom of the gasifier does not allow computing a sensible average value. All of the values show a sharp change in value at about the 4m. elevation where the upper injectors are located. At about the 11m. level (60% of the gasifier height), all of the values converge. Note that in the first stage, the centerline temperature is greater than the near wall gas temperature, but above the top injector the centerline temperature drops well below the near wall temperature. The overall decrease in gas temperature through the chamber is due to the endothermic reactions associated with gasification.

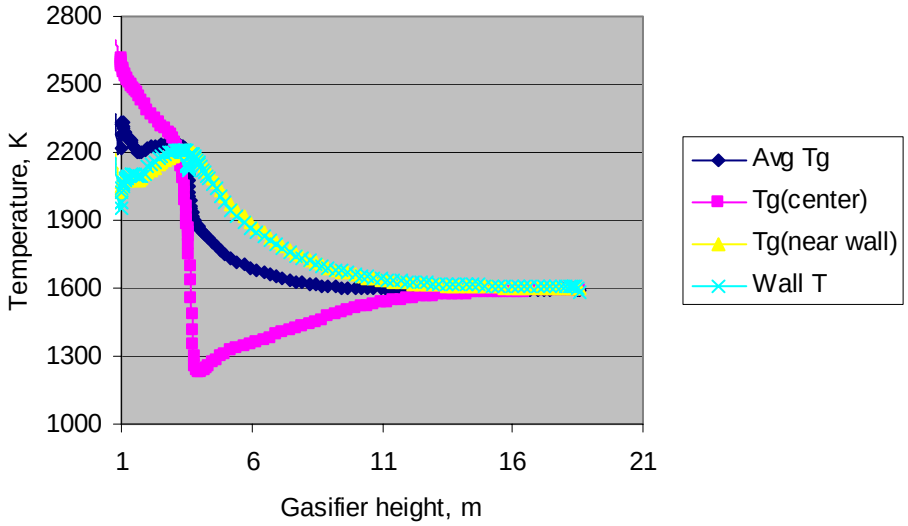

Figure 20. Two stage gasifier. Plotted as a function of axial position are the average gas temperature, centerline gas temperature, average gas temperature near the wall and the average wall temperature.

Illustrated in Figure 21 are XY plots for the gas composition along the gasifier axis. The plots indicate little change in the major species concentrations (on average) for the region between the top of the second level of injectors to just below the upper injectors. At the upper injectors the average composition shows a relatively sharp change for a short distance after which the values asymptote to their final values. There is little if any change in moisture concentration after the 12m. elevation, implying that little gasification occurs above this level. Comparing the plots of bulk, centerline and near-wall H2 gas concentration it can be seen that in the lower 50% of the gasifier, the local gas concentration exhibits more variations in value along the length of the gasifier than are observed by only looking at the bulk value.

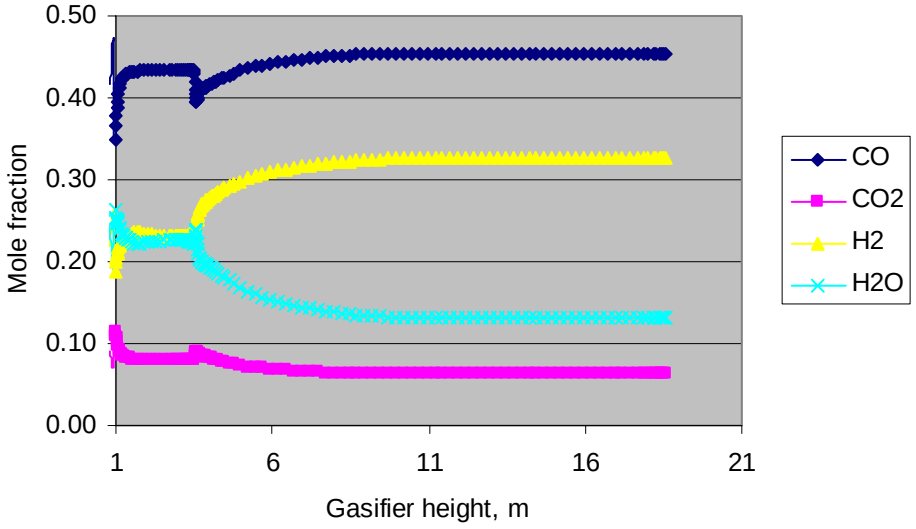

Figure 21a. Two stage gasifier. Plotted as a function of axial position are average concentration of major gas species.

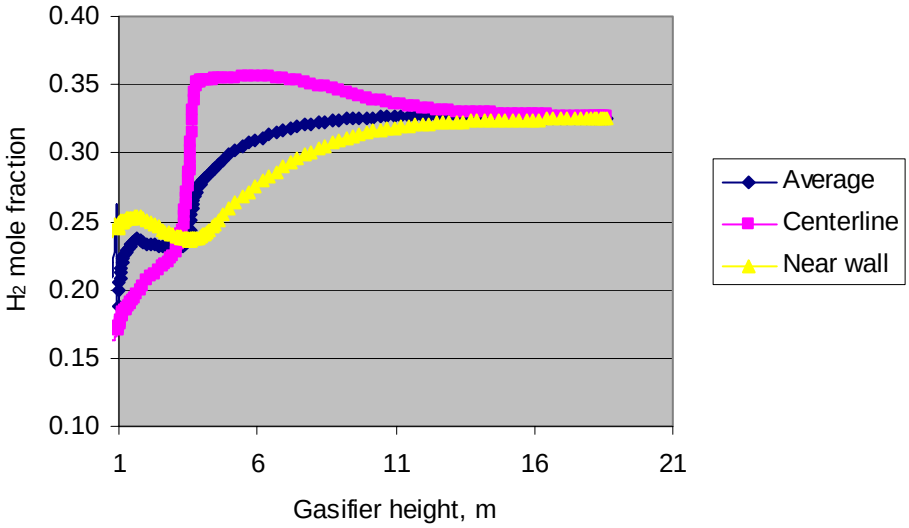

Figure 21b. One stage gasifier. Plotted as a function of axial position are average, centerline and near wall concentration of H_2.

Shown in Table 5 are the average values for the syngas quantity and composition at the gasifier exit. From the table it can be seen that for the baseline conditions the model predicts a high carbon conversion (over 99%), cold gas efficiency of slightly more than 87% and a syngas heating value of about 257 Btu/SCF. These values are much higher than that predicted for the single stage gasifier. A DOE funded study that employed an ASPEN analysis for an IGCC plant with a single stage gasifier [DOE-NETL, 2000b] predicted a normalized higher heating value of 250 Btu/SCF for comparable operating conditions as used in this simulation (same coal, slurry and oxidant flow rate, higher gasifier pressure and use flue gas recycle to temper exit temperature). Listed in the table are values for the residence times of the gas and fuel particles. For the given conditions and reactor volume this results in a PFR residence time of about 1.5 seconds. For fuel particles, the model predicts an average residence time of slightly less than one second. The strong swirling flow pattern provides the means to greatly increase the fuel residence time.

Table 5. Two Stage Gasifier Baseline

Exit Temperature, K	1594.9
Carbon Conversion, %	99.32
Exit LOI, %	1.48
PFR Residence Time, s	1.520
Particle Residence Time, s	0.996
Mole Fraction: CO	0.4541
H_2	0.3259
H_2O	0.1324
CO_2	0.0630
H_2S	0.0081
COS	0.0004
N_2	0.0154
Exit Mass Flow, klb/hr	502.18
HHV of Syngas, Btu/lb	5195.8
HHV of Syngas, Btu/SCF	257.2
Cold-Gas Efficiency, %	87.3

In the following we present numerical results for parametric studies that have been performed with the model. In general, there is relatively little visible change in plots of the gasifier flow field for the parametric cases. Hence, we present only tabulated values.

Effect of Average Fuel Particle Size

Fuel particle size is an important parameter for gasifier unit operation. In general, for coal combustion/gasification a finer grind (i.e., smaller mass mean particle size) reduces the time for combustion or gasification to occur. Hence for a fixed reactor chamber, more fuel conversion will occur. From a design viewpoint, the reduced time for fuel conversion would allow using a smaller (shorter) reactor and thereby potentially reduce cost. Pulverized coal is typically generated with a mill that uses parasitic power to operate. The finer the grind, the greater the parasitic power needs. Hence there is a trade-off that plant designer/operators must consider. Regardless of the fuel grind for which the gasifier is originally configured, particle size can (will) vary over time due to wear-and-tear on mills, equipment outages, etc..

Listed in Table 6 is a summary of the predicted gasifier performance for varying the fuel grind in the one stage gasifier. The three particle sizes modeled are mass mean particle sizes of 30, 40 and 60 microns, or 96%, 90% and 72% through 200 mesh, respectively. The assumption of a mass mean particle size of 40 microns for the baseline simulation is based on information from [Chen et al, 1999], [Chen et al, 2000]. As expected, the model predicts that increasing the average particle size decreases the carbon conversion, which results in an increase in exit gas temperature and lower heating value and cold gas efficiency. The increase in gas temperature is due to the sub-stoichiometric (fuel rich) conditions – that is less carbon conversion results in an oxygen fuel mixture that is slightly closer to stoichiometric and thus slightly hotter. The unburned carbon in the flyash (LOI) increases with increasing particle size. Although the different particle sizes resulted in about a 1% change in the syngas heating value, this change would be hard to identify by looking only at the syngas composition, which is quite similar for all three cases. Listed in Table 6 is a summary of the predicted gasifier performance for varying the fuel grind for the two-stage gasifier. The model predicts a very slight decrease in carbon conversion, heating value and cold gas efficiency. Although the expected trend is captured, the change in values are almost too small to be reliable.

Table 6. Effect of Particle Size

	One Stage			Two Stage		
Particle Size, μm	30.0	40.0	60.0	30.0	39.8	60.0
Exit Temperature, K	1889.0	1922.7	1953.6	1592.5	1594.9	1616.2
Carbon Conversion, %	97.91	97.15	95.63	99.45	99.32	98.78
Exit LOI, %	14.56	18.86	26.32	3.31	1.48	0.30
PFR Residence Time, s	0.661	0.653	0.635	1.523	1.520	1.505
Particle Resdience Time, s	0.919	0.996	0.027	0.919	0.996	1.037
Mole Fraction: CO	0.4232	0.4217	0.4170	0.4542	0.4541	0.4532
H_2	0.2452	0.2413	0.2350	0.3262	0.3259	0.3234
H_2O	0.2143	0.2192	0.2275	0.1320	0.1324	0.1357
CO_2	0.0905	0.0910	0.0935	0.0630	0.0630	0.0631
H_2S	0.0079	0.0079	0.0078	0.0081	0.0081	0.0081
COS	0.0005	0.0005	0.0005	0.0004	0.0004	0.0004
N_2	0.0182	0.0182	0.0184	0.0154	0.0154	0.0155
Exit Mass Flow, klb/hr	543.63	542.09	538.96	502.30	502.18	501.02
HHV of Syngas, Btu/lb	4178.8	4139.4	4058.5	5198.7	5195.8	5166.1
HHV of Syngas, Btu/SCF	225.2	223.7	218.1	257.3	257.2	256.3
Cold-Gas Efficiency, %	76.0	75.1	73.2	87.4	87.3	86.6

Effect of Slurry Pre-Heat

There should be an advantage to pre-heating the slurry fed to the gasifier. Use of a "cold" slurry feed requires that heat generated within the gasifier from the fuel conversion process be used to vaporize the liquid water used to transport the coal. As noted in [Holt, 2001a], pre-heating the slurry before injection into the gasifier should increase the thermal efficiency of the gasifier and thereby provide a means to increase the carbon conversion within the gasifier, or allow reducing the size of the gasifier if the same carbon conversion is desired. For systems with cold or warm gas clean-up, the slurry pre-heat can potentially be performed by passing the hot syngas exiting the gasifier through a heat exchanger that pre-heats the incoming cold slurry prior to injection to the gasifier. For the gasifier at the Polk Power Station there is no slurry pre-heat and the slurry enters the gasifier at ambient conditions (about 60 °F = 288 K). The gasifier at Wabash River uses a pre-heated slurry (about 350 °F = 450 K).

Listed in Table 7 is a summary of the predicted one stage performance using two different slurry-feed temperatures. The first case is for our baseline conditions in which a slurry pre-heat is used (slurry temperature = 422K). The second case, T = 278K, represents using ambient conditions, or no pre-heat. The model results indicate the desired trend on syngas production. Using slurry pre-heat results in increased carbon conversion, heating value and cold gas efficiency. Further studies are needed to determine if the magnitude of the improvement is reasonable.

Also listed in Table 7 is a summary of the predicted performance for the two stage gasifier performance for the same change in slurry feed temperatures. The predicted results are in effect the same, implying that for these conditions and geometry there would be no noticeable change in performance. When viewed with the results from the previous parametric test, it could be that we have selected a height for the gasifier that is sufficiently tall, or has a sufficiently long residence time, that the impact of operational changes is washed out by the exit of the gasifier.

Table 7. Effect of Slurry Pre-Heat

	One Stage		Two Stage	
Pre-Heat	Yes	No	Yes	NO
Slurry Temperature, K	422	298	422.0	298.0
Exit Temperature, K	1922.7	1860.7	1594.9	1595.5
Carbon Conversion, %	97.15	96.35	99.32	99.49
Exit LOI, %	18.86	22.99	1.48	1.34
PFR Residence Time, s	0.653	0.677	1.520	1.521
Mole Fraction: CO	0.4217	0.4159	0.4541	0.4544
H_2	0.2413	0.2411	0.3259	0.3260
H_2O	0.2192	0.2204	0.1324	0.1322
CO_2	0.0910	0.0957	0.0630	0.0628
H_2S	0.0079	0.0079	0.0081	0.0081
COS	0.0005	0.0005	0.0004	0.0004
N_2	0.0182	0.0183	0.0154	0.0154
Exit Mass Flow, klb/hr	542.09	540.44	502.18	502.34
HHV of Syngas, Btu/lb	4139.4	4092.9	5195.8	5199.7
HHV of Syngas, Btu/SCF	223.7	222.0	257.2	257.2
Cold-Gas Efficiency, %	75.1	74.0	87.3	87.4

Effect of Wet .vs. Dry Feed

The Texaco and E-Gas gasifiers used in the large scale IGCC plants in the USA (i.e., Polk Power, Wabash River and Eastman Chemical), all employ a water based slurry to transport the fuel into the gasifier chamber. In contrast, the gasifiers developed by Shell and by groups in Japan employ a dry feed system. Potential advantages to a dry feed system include greater cold gas efficiency and reduced oxygen requirements [Holt, 2001a]. The dry feed could be obtained by using nitrogen or possibly carbon-dioxide as a carrier gas. For IGCC plants using an oxygen blown gasifier the nitrogen stream can be obtained from the exhaust of the Air Separation Unit. Using nitrogen for the coal transport medium is not unique to coal gasification. Blast furnaces used in the steel industry employ nitrogen for coal transport through the coal injection lance located in the furnace tuyere.

Listed in Table 8 is a summary of the predicted performance for the one stage gasifier using wet and dry feed. In these tests, the wet feed case corresponds to the baseline simulation (coal-water slurry containing 74% solids) and the dry feed case employs nitrogen to transport the coal (0.1lb N2 per lb of coal). In both cases the fuel stream is assumed to be at the same temperature (T = 422K) and the coal is used "as received". For these simulations, the dry feed simulation shows only a small increase in carbon conversion. However, the syngas generated with the dry feed has a much higher mole fraction of CO. Likewise, the heating value of the syngas generated with dry feed is significantly greater than the heating value of the syngas generated by the wet feed. Although the syngas heating value increased for the dry feed, the lower syngas mass flow rate results in a slight reduction in the cold gas efficiency. In light of the substantial change in syngas composition between the different feeds, a potential question to address in future work would be the impact on downstream processes (e.g., gas clean up, gas turbines, fuel cells) due to using a dry feed.

Listed in Table 8 is a summary of the predicted performance for the two stage gasifier using wet and dry feed. For the two simulations, again, the carbon conversion is quite close. The dry feed indicates a slight reduction in carbon conversion. However, as with the one stage gasifier, due to injecting less moisture to the system the syngas produced with the dry feed has a much higher mole fraction of CO and heating value as compared to the wet feed simulation. In addition, due to the reduced mass flow of syngas, the dry feed results in a lower cold gas efficiency.

Table 8. Effect of Wet vs Dry Feed

	One Stage		Two Stage	
Feed Condition	Wet	Dry (N2)	Wet	Dry (N2)
Exit Temperature, K	1922.7	2361.2	1594.9	1831.1
Carbon Conversion, %	97.15	98.41	99.32	98.93
Exit LOI, %	18.86	11.54	1.48	0.97
PFR Residence Time, s	0.653	0.626	3.22	3.9
Mole Fraction: CO	0.4217	0.5670	1.52	1.591
H_2	0.2413	0.2268	0.4541	0.5936
H_2O	0.2192	0.0908	0.3259	0.3042
CO_2	0.0910	0.0403	0.1324	0.0141
H_2S	0.0079	0.0088	0.0081	0.0094
COS	0.0005	0.0009	0.0004	0.0007
N_2	0.0182	0.0630	0.0154	0.0599
Exit Mass Flow, klb/hr	542.09	481.57	502.18	437.92
HHV of Syngas, Btu/lb	4139.4	4626.1	5195.8	5890
HHV of Syngas, Btu/SCF	223.7	259.9	257.2	305.1
Cold-Gas Efficiency, %	75.1	74.6	87.3	86.3

Effect of System Pressure

From a modeling perspective, altering the system pressure for a fixed geometrical configuration is a useful parametric study to investigate model behavior. However, it is of limited value for practical operation. In the plant design process, the system pressure for the gasifier is determined by the amalgamation of considerations for the many equipment and processes to be used in the IGCC plant. Once the operating pressure for the gasifier is determined, the gasifier is sized to provide the desired fuel conversion for the anticipated residence time and conditions within the gasifier. Thus, in real world operation, one would not (and could not safely) significantly alter the steady state pressure from the original design condition. However, on the computer such tests can be performed.

Listed in Table 9 is a summary of the predicted performance for the one stage gasifier for varying the system pressure within the gasifier. The selected pressures are 18, 30 and 70 atm. and correspond to (a) the baseline conditions for our Vision 21 reference condition, (b) approximately the system pressure used by current generation coal gasifiers used for power production (and for many DOE IGCC studies) and (c) approximately the pressure reported for coal gasifiers used at "coal-to-chemicals" plants. From the table it appears that the model predicts the expected trends. As the system pressure increases the average gas residence time increases due to the reduced average gas velocity. The slower gas velocities result in increased particle residence time which in turn results in increased carbon conversion. At 70 atm., the model predicts in effect complete conversion of the fuel. It is interesting to note that in this study the pressure was increased by almost a factor of four, but the syngas higher heating value and cold gas efficiency only increased by a few percentage points. Listed in Table 9 is a summary of the predicted performance for the two-stage gasifier for the same set of system pressures. From the table it appears that the model predicts the expected trends. As the system pressure increases the average gas residence time increases due to the reduced average gas velocity. The slower gas velocities result in increased particle residence time which in turn results in increased carbon conversion. At 70 atm., the model predicts in effect complete conversion of the fuel.

Table 9. Effect of Pressure

	One Stage			Two Stage		
Pressure, atm	18	30	70	18	30	70
Exit Temperature, K	1922.7	1905.5	1934.6	1594.9	1590.7	1619.7
Carbon Conversion, %	97.15	98.95	99.99	99.32	99.65	99.85
Exit LOI, %	18.86	7.90	0.04	1.48	1.14	0.32
PFR Residence Time, s	0.653	1.093	2.512	1.520	2.540	5.881
Particle Residence Time, s	0.026	0.042	0.101	0.996	1.405	2.910
Mole Fraction: CO	0.4217	0.4276	0.4324	0.4541	0.4548	0.4563
H_2	0.2413	0.2481	0.2505	0.3259	0.3261	0.3231
H_2O	0.2192	0.2100	0.2062	0.1324	0.1312	0.1327
CO_2	0.0910	0.0876	0.0842	0.0630	0.0628	0.0616
H_2S	0.0079	0.0079	0.0080	0.0081	0.0082	0.0082
COS	0.0005	0.0005	0.0005	0.0004	0.0004	0.0004
N_2	0.0182	0.0181	0.0180	0.0154	0.0154	0.0154
Exit Mass Flow, klb/hr	542.09	545.77	547.90	502.18	502.90	503.29
HHV of Syngas, Btu/lb	4139.4	4234.0	4290.3	5195.8	5210.7	5217.8
HHV of Syngas, Btu/SCF	223.7	227.6	230.0	257.2	257.6	257.8
Cold-Gas Efficiency, %	75.1	77.3	78.7	87.3	87.7	87.9

Effect of Reaction Kinetics for Same Fuel

As discussed in the previous section on reaction kinetics (see above), the choice in reaction kinetics can have a significant impact on predicted values for a computational model. This can be especially important if computational models are used to help guide the sizing and design of gasification equipment. Unfortunately, there remains much work to be performed to establish reliable, general purpose rules and correlations that analysts can use to estimate kinetic parameters for different coals for gasification applications.

To demonstrate the impact of using different kinetics, in this section we compare solutions predicted using two kinetic sets from the literature. The tests are performed using kinetic parameters developed by [Lupa and Kliesh, 1979] and [Roberts and Harris, 2000]. The kinetic parameters by [Lupa and Kliesh, 1979] were developed for Illinois #6 coal across a range of temperatures and pressures representative of gasification conditions. These are the same kinetic parameters as used in the baseline simulation. The kinetic parameters taken from [Roberts and Harris, 2000] are for an Australian coal (coal Y) with properties comparable to Illinois #6, for tests performed at 10 atm.. Comparing the two sets of kinetics, for high temperatures and pressures the two kinetic sets are comparable for combustion ($C+O_2$) reactions but for gasification reactions ($C+CO_2$, $C+H_2O$) the baseline kinetic set is at least an order of magnitude faster than that of [Roberts and Harris, 2000].

Listed in Table 10 is the predicted performance for the one stage gasifier for using the two sets of kinetic parameters. In this test, the coal kinetics were the only model input parameters changed. Comparing the simulation results, it can be seen that the two parameter sets predict very different behavior. Using the parameters by Roberts and Harris results in a significantly lower carbon conversion. As a result, the carbon-in-ash (LOI) is much higher and the syngas mass flow rate, heating value and cold gas efficiency are much lower.

Listed in Table 10 is the predicted performance for the two-stage gasifier using the two sets of kinetic parameters. The impact of the different kinetics is not as severe for this gasifier as it was

Table 10. Effect of kinetics

	One Stage		Two Stage	
Reaction Kinetics Set	Lupa and Kliesh	CCSD	Lupa and Kliesh	CCSD
Exit Temperature, K	1922.7	2135.5	1594.9	1759.8
Carbon Conversion, %	97.15	84.93	99.32	94.01
Exit LOI, %	18.86	55.13	1.48	30.80
PFR Residence Time, s	0.653	0.647	1.520	1.441
Mole Fraction: CO	0.4217	0.3772	0.4541	0.4434
H_2	0.2413	0.1900	0.3259	0.3036
H_2O	0.2192	0.2886	0.1324	0.1625
CO_2	0.0910	0.1159	0.0630	0.0662
H_2S	0.0079	0.0066	0.0081	0.0080
COS	0.0005	0.0005	0.0004	0.0004
N_2	0.0182	0.0195	0.0154	0.0158
Exit Mass Flow, klb/hr	542.09	517.16	502.18	491.54
HHV of Syngas, Btu/lb	4139.4	3461.1	5195.8	4916.8
HHV of Syngas, Btu/SCF	223.7	195.3	257.2	246.8
Cold-Gas Efficiency, %	75.1	59.9	87.3	80.9

for the one stage configuration. Using the parameters by Roberts and Harris results in a noticeably lower carbon conversion. As observed in other simulations, the lower carbon conversion results in a higher exit gas temperature. Compared to the baseline, the LOI is much higher and the syngas mass flow rate, temperature, heating value and cold gas efficiency are much lower.

The results of this parametric test emphasize the importance of using the best available reaction kinetics.

Effect of Fuel Switching

The economics of operating an IGCC plant require that the operator have the flexibility to switch fuels and maintain good gasifier performance. As an example, the Polk Power Station has operated with over twenty different solid fuels since startup [Hornick, 2002]. However fuel switching is not a trivial process. The new fuel must maintain the required syngas production and good slagging properties must be maintained to protect the refractory from excessive wear.

Gasifier simulations have been performed using three different solid fuels: Illinois #6, Power River Basin (PRB) and Petcoke. All three fuels have been used in commercial scale gasifiers. The Petcoke and PRB are popular in some regions of the USA due to their low price. All three simulations were performed using the same model inputs, excepting for fuel composition (see Table 3) and kinetic parameters. The kinetic parameters for Illinois #6 are the same as used in the baseline simulation [Lupa and Kliesh, 1979]. The kinetics for Petcoke were estimated by using the values from Lupa and Kliesch and reducing these by a factor of five. The kinetic parameters for PRB were estimated in a similar manner, but by multiplying by a factor of five.

Table 11. Effect of Fuel Type - One Stage Only

Fuel Type	Illinois#6	Petcoke	PRB
Exit Temperature, K	1922.7	2327.3	1700.7
Carbon Conversion, %	97.15	99.38	91.40
Exit LOI, %	18.86	52.28	54.15
PFR Residence Time, s	0.653	0.562	0.754
Mole Fraction: CO	0.4217	0.4991	0.3521
H_2	0.2413	0.2180	0.2246
H_2O	0.2192	0.1782	0.2738
CO_2	0.0910	0.0734	0.1297
H_2S	0.0079	0.0096	0.0016
COS	0.0005	0.0008	0.0001
N_2	0.0182	0.0177	0.0181
Exit Mass Flow, klb/hr	542.09	546.63	530.39
HHV of Syngas, Btu/lb	4139.4	4294.5	3535.0
HHV of Syngas, Btu/SCF	223.7	240.4	195.1
Cold-Gas Efficiency, %	75.1	75.0	71.0

Listed in Table 11 is the predicted gasifier performance for the three fuels. Comparing the results it can be seen that the different fuels produce syngas with quite different compositions, quality, heating value and cold gas efficiency. Relative to the performance of Illinois #6 (baseline), the Petcoke resulted in higher carbon conversion. The LOI of the flyash appears high due to the very small amount of ash in the Petcoke making any carbon in the flyash appear as a large LOI value. Compared to the baseline, the Petcoke resulted in a significantly higher exit temperature due to the high amount of carbon and relatively few dilatants in Petcoke. The predicted CO concentration in the syngas generated by Petcoke is much higher than that for Illinois #6. Likewise, the predicted heating value (Btu/SCF) for Petcoke is noticeably greater than for Illinois #6. However, the cold gas efficiency

is lower than for Illinois #6 due to the much higher heating value of Petcoke in as received form. Comparing the predicted values for the Illinois # 6 and PRB, the syngas generated with PRB has somewhat lower carbon conversion, and a noticeably lower CO concentration, heating value and cold gas efficiency.

The results of this test should not be interpreted to indicate that one fuel might be better than another for gasifier applications. Such a comparison will require a more in-depth analysis than performed here. In particular, more thought needs to be invested on how to modify the operating conditions (e.g., oxygen and steam flows) to match the syngas produced for the baseline operation. With such a comparison, then the criteria to judge the benefit (if any) of using different fuels could be limited to the differential cost to operate at the required conditions and the impact on slag management and refractory wear.

Effect of Gasifier Length

An advantage to using computational models is that it provides a means to "easily" explore the impact on performance of altering the size, shape or volume of the gasifier.

Listed in Table 12 is the predicted gasifier performance for the baseline configuration and two alternative gasifier sizes. For simplicity, in this study we only change the gasifier length. The three simulations correspond to the gasifier having a L/D ratio = 1, 2 (baseline) and 3. Comparing the predicted values, the expected trends are observed. As the gasifier increases in length, the predicted carbon conversion, mean particle residence time, syngas heating value and cold gas efficiency increase correspondingly. In addition, note that for L/D=1, the predicted carbon conversion is in excess of 90% suggesting that most of the fuel conversion happens very rapidly within the gasifier.

Table 12. One Stage Gasifier – Effect of length

Gasifier Length (L/D ratio)	1	2 (baseline)	3
Exit Temperature, K	2021.9	1922.7	1870.2
Carbon Conversion, %	92.72	97.15	99.27
Exit LOI, %	37.25	18.86	5.41
PFR Residence Time, s	0.332	0.653	0.969
Mole Fraction: CO	0.4081	0.4217	0.4274
H_2	0.2232	0.2413	0.2506
H_2O	0.2429	0.2192	0.2071
CO_2	0.0984	0.0910	0.0882
H_2S	0.0074	0.0079	0.0079
COS	0.0005	0.0005	0.0005
N_2	0.0187	0.0182	0.0180
Exit Mass Flow, klb/hr	532.72	542.09	546.42
HHV of Syngas, Btu/lb	3906.5	4139.4	4249.7
HHV of Syngas, Btu/SCF	212.7	223.7	228.0
Cold-Gas Efficiency, %	69.7	75.1	77.7

SUMMARY

In this paper we have described a CFD based model for entrained flow coal gasifiers. The model contains sub-models to properly model the reaction kinetics of coal gasification at high pressure, high solids loading and slagging walls. Two gasifier configurations have been used for test cases: (1) a single stage, down fired system and (2) a two stage system with multiple feed inlets that could be opposed or tangentially fired. These systems are representative of the dominant, commercially available gasifier systems. Simulations results have been presented for a baseline conditions and a series of off-design or "what if" scenarios to highlight the sensitivity of the model to key parameters. Although the models have been demonstrated for oxygen blown, pressurized systems the same model could be applied to air-blown or atmospheric systems. The emphasis in this paper has been to document the capabilities of the model. The results from the simulations presented here should not be interpreted to mean one gasifier configuration is "better" than the other. Future work will focus on investigating using the model to improve the operation and design of entrained flow gasifiers.

ACKNOWLEDGEMENT

Funding for this program has been provided by the DOE Vision 21 Program (DE-FC26-00FNT41047, DOE-NETL Project Manager: John Wimer). We would like to thank Neville Holt (EPRI) for the many useful discussions we have had on gasification systems. In addition, we would like to thank Prof. Terry Wall, Prof. John Kent, Dr. David Harris, Mr. Peter Benyon and their many colleagues at the Collaborative Research Center for Coal and Sustainable Development (CCSD) in Australia for providing access to data, reports and manuscripts on their research into coal gasification.

REFERENCES

Adams, B.R., et al, eds. *Technical Overview of Reaction Engineering International Combustion Simulation Software,* Reaction Engineering International, SLC, UT, 1995.

Anthony D.B. and Howard J.B., Coal devolatilization and hydrogasification, *AIChE J*., **22,** 625-656, 1976.

Arendt P. and van Heek K.H., Comparative investigations of coal pyrolysis under inert gas and H_2 at low and high heating rates and pressures up to 10 MPa, *Fuel*, **60,** 779-787, 1981.

Banin et al., *Combustion and Flame*, **108**, 1-8, 1997.

Beath A.C., Mathematical modeling of entrained flow gasification, PhD thesis, University of Newcastle, Australia, 1996.

Benfell, K. E., Liu, G.-S., Roberts, D. G., Harris, D. J., Lucas, J. A., Bailey, J. D., and Wall, T. F., *Proceedings of the Combustion Institute,* **28**, 2233-2241, 2000.

Benyon, P., Inumaru, J., Otaka, M., Hara, S., Watanabe, H. and Kent J. Engineering Modelling of High Pressure and Temperature Entrained-Flow Gasifiers. *Japan-Australia Joint Technical Meeting on Coal*, December 5-6, 2000, Fukuoka, Japan.

Benyon P.J., Computational modeling of entrained flow slagging gasifiers, PhD thesis, University of Sydney, Australia, 2002.

Bockelie, M.J., Adams, B.R., Cremer, M.A., Davis, K.A., Eddings, E.G., Valentine, J.R., Smith, P.J., and Heap, M.P., Computational simulations of industrial furnaces, Proceedings of the International Symposium on Computational Technologies For Fluid/Chemical Systems with Industrial Applications, Joint ASME/JSME Conference, San Diego, CA, 1998.

Bockelie, M.J., Swensen, D.A., Denison, M.K., Chen, Z., Senior, C.L., Sarofim, A.F., A Computational Workbench Environment for Virtual Power Plant Simulation, *Proceedings of the 27th International Technical Conference on Coal Utilization and Fuel Systems*, Clearwater, FL, USA, March 4-7, 2002.

CCSD. URL = http://www.newcastle.edu.au/research/centres/blackcoal.html.

Chen, C. Miyoshi, T., Kamiya, H., Horio, M., and Kojima, T., On the Scaling-up of a Two-Stage Air Blown Entrained Flow Coal Gasifier, *The Canadian Journal of Chemical Engineering*, **77**, 745-750, 1999.

Chen, C., Horio, M., and Kojima, T., Numerical Simulation of Entrained Flow Coal Gasifiers, *Chemical Engineering Science*, **55,** 3861-3883, 2000.

DOE-NETL, Texaco Gasifier IGCC Base Cases, PED-IGCC-98-001, July 1998, Latest Revision, June 2000a.

DOE-NETL, DESTEC Gasifier IGCC Base Cases, PED-IGCC-98-003, September 1998, Latest Revision, June 2000b.

Fletcher T.H., Kerstein A.R., Pugmire R.J. and Grant D.M., *Energy & Fuels*, **4**, 54, 1990.

Gibbins J.R. and Kandiyoti R., The effect of variations in time-temperature history on product distribution from coal pyrolysis, *Fuel*, **68,** 895-903, 1989.

Griffin T.P., Howard J.B. and Peters W.A., Pressure and temperature effects in bituminous coal pyrolysis: experimental observations and a transient lumped-parameter model, *Fuel*, **73**, 591-601, 1994.

Harris D.J., Kelly M.D., Roberts D.G., Mill C.J., Stubington J.F. and Wall T.F., Determining coal reactivity parameters at elevated pressures using bench-scale techniques, 2002.

Harris, D. J., and Smith, I. W., *Proceedings of the Combustion Institute*, **23**, 1185-1190, 1990.

Holt, N., Integrated Gasification Combined Cycle Power Plants, unpublished manuscript, March, 2001a.

Holt, N., Coal Gasification Research, Development and Demonstration – Needs and Opportunities, presented at the *Gasification Technologies 2001 Conference*, San Francisco, CA, Oct. 8-10, 2001b.

Hornick, M., Polk Power Station IGCC, *Proceedings of the 27th International Technical Conference on Coal Utilization and Fuel Systems*, Clearwater, FL, USA, March 4-7, 2002.

Hoy, H.R., Roberts, A.G. and Wilkins, D.M., Behavior of mineral matter in slagging gasification processes. *J. Inst. Gas Engrs,* **5**, 444, 1965.

Hurt, R., Sun, J-K, Lunden, M., *Combustion and Flame,* **113**, 181, 1998.

IEA, *Modeling and Simulation for Coal Gasification*, IEA Coal Research 2000, ISBN 92-9029-354-3, December, 2000.

Joutsenoja et al., *Energy and Fuels*, **13**, 130-145, 1999.

Kobayashi, H., Howard, J.B. and Sarofim, A.F., Coal devolatilization at high temperatures, *6th Symposium (Int) on Combustion*, The Combustion Institute, 411-425, 1976.

Liu, G., Benyon, P., Benfell, K.E., Bryant, G.W., Tate, A.G., Boyd, R. K., Harris, D.J., and Wall, T.F., *Fuel*, **79**, 617-626, 2000.

Lupa and Kliesch, Simulation of a Texcao Gasifier, Vol.1 A Steady State Model, EPRI Report AF-1179, Vol. 1 Research Project 1037-1. Final Report, 1979.

Monson et al., *Combustion and Flame*, **100**, 669-683, 1995.

Niksa S. and Kerstein A.R., FLASHCHAIN theory for rapid coal devolatilization kinetics 1. Formulation, *Energy & Fuels*, **5**, 673-683, 1991.

NRC, *Coal - Energy for the Future*, National Academy Press, Washington, DC, 1995.

Okumura Y., Sugiyama Y. and Okazaki K., Evolution behavior of coal-nitrogen in high pressure pyrolysis processes, *Fuel Chemistry Division Preprints*, **46**, 141-143, 2001.

Otaka et al., the 26th International Conference on Coal Utilization and Fuel Systems, Clearwater, Fl., 2001.

Patterson, J.H. Hurst, H.J. Quintanar, A. Boyd, B.K. and Tran, H. Evaluation of the slag flow characterization of Australian coals in slagging gasifiers. *Research Report 19, Volume 1. Cooperative Research Centre for Black Coal Utilisation*, University of Newcastle, Australia, May, 2001.

REI_Models. URL http://www.reaction-eng.com.

Roberts, D.G. and Harris, D.J., Char gasification with O2, CO2, and H2O: Effects of pressure on intrinsic reaction kinetics, *Energy & Fuels*, **14**, 483-489, 2000.

Roberts, D.G., Harris, D. J., and Wall, T. F., High-Pressure Intrinsic Char Gasification Kinetics: an Application of a modified nth-order rate equation, the 18th Pittsburgh Coal Conference, Newcastle, Australia, 3-7 Dec, 2001.

Rodgers, M.W., Slag layers in coal-fired MHD generators. *PhD thesis*, Stanford University, Palo Alto, CA, 1979.

Seggiani, M., Modelling and simulation of the time varying slag flow in a Prenflo entrained-flow gasifier. *Fuel*, **77**, 1611, 1998.

Senior, C.L. and Sangiovanni, J.J., Numerical model of slag flow in a novel coal-fired furnace, *International Journal of Heat and Mass Transfer*, 2001.

Senneca, O., Salatino, P., Masi, S., *Fuel*, **77**, 1483, 1998.

Smith I.W., The combustion rates of coal chars: a review, *Proceedings of the Combustion Institute*, 1045-1065, 1982.

Smoot, L.D. and Smith, P.J., *Coal Combustion and Gasification*, Plenum Press, NY, NY 1985.

Solomon P.R., Hamblen D.G., Carangelo R.M., Serio M.A. and Deshpande G.V., General model of coal devolatilization, *Energy & Fuels*, **2**, 405, 1988.

Solomon P.R., Serio M.A. and Suuberg E.M., Coal pyrolysis: experiments, kinetic rates and mechanisms, *Prog. Energy Combustion Sci*., **18**, 133-220, 1992.

Steigel, G.J., Clayton, S.J., and Wimer, J.G., DOE's Gasification Industry Interviews: Survey of Market Trends, Issues, and R&D Needs, presented at the *Gasification Technologies 2001 Conference*, San Francisco, CA, Oct. 8-10, 2001.

Suuberg E.M., Peters W.A. and Howard J.B., Product compositions and formation kinetics in rapid pyrolysis of pulverised coal - implications for combustion, *Proceedings of the Combustion Institute*, **17,** 117-128, 1978.

Urbain, G., Cambier, F., Deletter, M., and Anseau, M.R., Viscosity of Silicate Melts. *Trans. J. Br. Ceram. Soc.*, **80**, 139, 1981.

Wall T.F., Liu G.-S., Wu H.-W., Roberts D.G., Benfell K.E., Lucas J.A. and Harris D.J., The effect of pressure on coal reactions during pulverized coal combustion and gasification, to be published, 2002.

Watt, J.D., The flow properties of slags formed from the ashes of British coals: Part 2. The crystallizing behavior of the slags. *J. Inst. Fuel*, **42**, 131, 1969.

Wen C.Y. and Chaung T.Z., Entrained coal gasification modeling, *Ind. Eng. Chem. Process Des. Dev.,* **18**, 684-695, 1979.

Wu, H., Bryant, G. W., and Wall, T. F., *Energy and Fuels*, **14**, 745-750, 2000.